Table 1a (*continued*)

GenBank ID	slr—Average	slr—S.D.	Gene-information
Others and non-classified (21)			
X02801	1	0.53	glial fibrillary acidic protein
D85785	0.92	0.07	protein tyrosine phosphatase, non-receptor type substrate 1
U75321	0.72	0.32	ATPase, aminophospholipid transporter (APLT), class I, type 8A, member 1
AF042180	0.67	0.17	testis-specific protein, Y-encoded-like
AW124835	0.59	0.05	similar to *S*-adenosylmethionine synthetase gamma form (Methionine adenosyltransferase) (AdoMet synthetase) (MAT-II)
AI835481	0.57	0.15	beta-1,3-glucuronyltransferase 3 (glucuronosyltransferase I)
AB033168	0.56	0.23	ZAP3 protein
U51167	0.56	0.03	isocitrate dehydrogenase 2 (NADP+), mitochondrial
X66091	0.54	0.08	*M. musculus* ASF mRNA
AW212859	−0.53	0.12	axotrophin
AI843662	−0.53	0.2	stromal membrane-associated protein
AW046672	−0.53	0.08	DNA segment, Chr 11, ERATO Doi 603, expressed
L00993	−0.53	0.13	Sjogren syndrome antigen B
AW124329	−0.54	0.14	RIKEN cDNA 4921531G14 gene
AI844469	−0.56	0.13	RIKEN cDNA 0610012D09 gene
M34896	−0.56	0.14	ecotropic viral integration site 2
U95498	−0.67	0.22	ALL1-fused gene from chromosome 1q

of zero would indicate no change. Categorization was based on the NetAffx database (http://www.NetAffx.com) [22]. For unsupervised, hierarchical cluster analysis, the Genesis software was used [39].

3. Results

In order to gain insight into the complex expression pattern of mice with a disturbed protein degradation pathway, microarrays representing 12,000 genes were hybridized with labelled RNA isolated from whole brain tissue of 3-month-old male gad mice and compared to two wildtype littermates of the same age. Thus, six comparisons of the expression pattern were achieved. The complete raw data set is publicly available and can be requested directly from the authors. We called a gene (a) stringent differentially regulated when at least six of the six comparisons revealed similar results or (b) moderate differentially regulated when five of six comparisons showed similar results. For both stringencies, genes with an expression difference of at least 1.4-fold (Signal Log Ratio of 0.5) between gad and wildtype mice were considered as significant.

The criteria for stringent differentially regulated genes (Table 1a) were fulfilled by 76 genes with known or putative function and by four ESTs with unknown function. Fifty seven of the genes were up-regulated, whereas

Table 1b
List of moderate differentially regulated genes

GenBank ID	slr—Average	slr—S.D.	Gene-information
RNA-metabolism (4)			
AA791742	1.09	0.28	ARP2 actin-related protein 2 homolog (yeast)
AA690583	0.87	0.34	splicing factor proline/glutamine rich (polypyrimidine tract binding protein associated)
U93050	0.77	0.43	poly(A) binding protein, nuclear 1
AI843586	0.72	0.21	splicing factor, arginine/serine rich 9 (25 kDa)
Vesicle-transport-proteins (4)			
U60150	0.8	0.24	vesicle-associated membrane protein 2
AB025218	0.71	0.11	coated vesicle membrane protein
D12713	0.68	0.15	SEC23A (*S. cerevisiae*)
U91933	0.64	0.3	adaptor-related protein complex AP-3, sigma 2 subunit
Cellular structure proteins (6)			
AF067180	1	0.16	kinesin family member 5C
U51204	0.6	0.19	expressed sequence AI790651
AB023656	0.6	0.21	kinesin heavy chain member 1B
M21041	0.73	0.21	microtubule-associated protein 2
X61399	0.69	0.4	MARCKS-like protein
M18775	−0.69	0.22	microtubule-associated protein tau
Channel-proteins (10)			
X78874	0.81	0.19	chloride channel 3
X16645	0.74	0.28	ATPase, Na+/K+ transporting, beta 2 polypeptide
U43892	0.7	0.16	ATP-binding cassette, subfamily B (MDR/TAP), member 7
U14419	0.67	0.14	gamma-aminobutyric acid (GABA-A) receptor, subunit beta 2
Y17393	0.66	0.24	prefoldin 2
U16959	0.65	0.15	FK506 binding protein 5 (51 kDa)
D10028	0.55	0.2	glutamate receptor, ionotropic, NMDA1 (zeta 1)
D50032	0.51	0.2	trans-golgi network protein 2
U73625	0.51	0.11	transient receptor potential cation channel, subfamily C, member 1
Defense (3)			
X06454	0.73	0.24	complement component 4 (within H-2S)
AW050268	0.64	0.19	HLA-B associated transcript 2
X66295	0.53	0.11	complement component 1, q subcomponent, c polypeptide
Lipid-metabolism (3)			
M91458	−0.53	0.7	sterol carrier protein 2, liver
AB017026	−0.54	0.19	oxysterol binding protein-like 1A
AI845798	−0.6	0.35	RIKEN cDNA 2310004B05 gene
Ca-metabolism (2)			
X87142	0.83	0.33	calcium/calmodulin-dependent protein kinase II alpha
AI842328	0.82	0.58	calmodulin 3
Growth factors (2)			
U42384	−0.65	0.25	fibroblast growth factor inducible 15
X55573	−0.73	0.23	brain-derived neurotrophic factor

(continued on next page)

Table 1b (*continued*)

GenBank ID	slr—Average	slr—S.D.	Gene-information
Chromatin-structure (2)			
M25773	0.7	0.33	SWI/SNF related, matrix associated, actin-dependent regulator of chromatin, subfamily d, member 1
AA794509	0.64	0.27	SWI/SNF-related, matrix-associated, actin-dependent regulator of chromatin, subfamily a, member 5
Chaperones (2)			
D85904	−0.56	0.16	heat shock 70 kDa protein 4
M20567	0.97	0.31	heat shock protein, 70 kDa 2
Signal transduction (25)			
U50413	1.53	0.92	phosphatidylinositol 3-kinase, regulatory subunit, polypeptide 1 (p85 alpha)
AF077660	1.26	0.23	homeodomain interacting protein kinase 3
AF022992	1.04	0.13	period homolog 1 (*Drosophila*)
AI838022	0.89	0.31	ADP-ribosylation factor 3
M63659	0.88	0.46	guanine nucleotide binding protein, alpha 12
U29055	0.77	0.32	guanine nucleotide binding protein, beta 1
AI849333	0.75	0.17	cerebellar postnatal development protein 1
X84239	0.74	0.14	RAB5B, member RAS oncogene family
AW125157	0.7	0.1	F-box and WD-40 domain protein 1B
AB005654	0.7	0.14	mitogen-activated protein kinase kinase 7
AI645561	0.69	0.28	NMDA receptor-regulated gene 1
M97516	0.69	0.11	
AA822412	0.68	0.27	RIKEN cDNA 2610313E07 gene
AF001871	0.66	0.13	pleckstrin homology, Sec7 and coiled/coil domains 3
AA982714	0.64	0.36	adrenergic receptor kinase, beta 1
AF054623	0.62	0.17	frizzled homolog 1, (*Drosophila*)
D87902	0.62	0.17	ADP-ribosylation factor 5
AF014371	0.61	0.18	ras homolog gene family, member A2
AI450876	0.59	0.17	*Mus musculus*, similar to pyridoxal kinase, clone MGC:29261 IMAGE:5064695, mRNA, complete cds
AJ001418	0.57	0.1	pyruvate dehydrogenase kinase, isoenzyme 4
L25674	0.56	0.19	nuclear receptor subfamily 2, group F, member 6
AI840130	−0.56	0.15	Src activating and signaling molecule
AV280750	−0.56	0.14	mitogen-activated protein kinase 10
U20238	−0.56	0.12	RAS p21 protein activator 3
AV370035	−0.73	0.23	chemokine (C–C) receptor 5
Protein degradation (12)			
AW125800	1.18	0.35	ESTs, weakly similar to ubiquitin specific protease 8; putative deubiquitinating enzyme [*Mus musculus*] [*M. musulus*]
L21768	0.83	0.13	epidermal growth factor receptor pathway substrate 15

Table 1b (*continued*)

GenBank ID	slr—Average	slr—S.D.	Gene-information
Protein degradation (12)			
AI853269	0.66	0.27	proteasome (prosome, macropain) subunit, beta type 2
X57349	0.65	0.11	transferrin receptor
M97216	0.59	0.28	amyloid beta (A4) precursor-like protein 2
AW050342	0.5	0.09	ubiquitin specific protease 21
AI849361	−0.54	0.12	RIKEN cDNA 1700056O17 gene
AI838853	−0.59	0.08	ubiquitin carboxyl-terminal esterase L5
AI839363	−0.65	0.17	eukaryotic translation initiation factor 3, subunit 6 48-kDa
AI846787	−0.67	0.22	Vhlh-interacting deubiquitinating enzyme 1
AI842835	−0.7	0.09	RIKEN cDNA 1500004O06 gene
AI839225	−0.86	0.17	leucine aminopeptidase 3
Membran-transport (5)			
AF064748	1.56	0.7	plasma membrane associated protein, S3–12
M22998	1.13	0.27	solute carrier family 2 (facilitated glucose transporter), member 1
AB035174	1.03	0.48	sialytransferase 7 ((alpha-*N*-acetylneuraminyl 2,3-betagalactosyl-1,3)-*N*-acetyl galactosaminide alpha-2, 6-sialytransferase) F
M75135	0.89	0.32	solute carrier family 2 (facilitated glucose transporter), member 3
AI843448	0.84	0.36	microsomal glutathione *S*-transferase 3
Transcription-regulation (22)			
M36514	1.19	0.26	zinc finger protein 26
AB021491	0.92	0.32	staphylococcal nuclease domain containing 1
M88299	1.11	0.5	
M61007	0.96	0.23	CCAAT/enhancer binding protein (C/EBP), beta
M62362	0.81	0.04	CCAAT/enhancer binding protein (C/EBP), alpha
AF015881	0.73	0.13	
AI850638	0.65	0.13	thyrotroph embryonic factor
U47543	0.62	0.23	Ngfi-A binding protein 2
AF064553	0.58	0.25	nuclear receptor-binding SET-domain protein 1
AF084480	0.54	0.19	bromodomain adjacent to zinc finger domain, 1B
X61800	0.51	0.14	CCAAT/enhancer binding protein (C/EBP), delta
X72310	−0.5	0.18	transcription factor Dp 1
L10426	−0.52	0.24	ets variant gene 1
D38046	−0.55	0.19	topoisomerase (DNA) II beta
U16322	−0.56	0.1	transcription factor 4
U07861	−0.59	0.15	zinc finger protein 101
AF034745	−0.63	0.17	ligand of numb-protein × 1
Z67747	−0.65	0.13	zinc finger protein 62
AI843959	−0.66	0.25	RIKEN cDNA 5730403B10 gene
AI957030	−0.66	0.33	RIKEN cDNA 2310001H12 gene
AI851230	−0.76	0.12	RIKEN cDNA 2310035M22 gene
X94127	−0.94	0.14	SRY-box containing gene 2

Table 1b (*continued*)

GenBank ID	slr—Average slr	—S.D.	Gene-information
Others and non-classified (44)			
AI851703	1.31	0.47	expressed sequence AW049671
AW227650	1.25	0.26	RIKEN cDNA 0610038P07 gene
AI877157	1.21	0.41	transmembrane 4 superfamily member 9
AF058799	1.14	0.31	3-monooxgenase/tryptophan 5-monooxgenase activation protein, gamma polypeptide
X02801	1	0.53	glial fibrillary acidic protein
D85785	0.92	0.07	protein tyrosine phosphatase, non-receptor type substrate 1
M93310	0.86	0.76	metallothionein 3
U52824	0.81	0.17	tubby
AI646638	0.79	0.15	*Mus musculus*, clone MGC:37615 IMAGE:4989784, mRNA, complete cds
AF006466	0.79	0.03	formin-like
AW227650	0.77	0.22	RIKEN cDNA 0610038P07 gene
U75321	0.72	0.32	ATPase, aminophospholipid transporter (APLT), class I, type 8A, member 1
AF039833	0.69	0.39	contactin associated protein 1
AF042180	0.67	0.17	testis-specific protein, Y-encoded-like
U62673	0.62	0.12	
AI849718	0.6	0.2	RIKEN cDNA 1500010B24 gene
AA414964	0.6	0.2	ESTs, Weakly similar to ATY1_MOUSE Probable cation-transporting ATPase 1 [*M. musulus*]
AW124835	0.59	0.05	similar to *S*-adenosylmethionine synthetase gamma form (Methionine adenosyltransferase) (AdoMet synthetase) (MAT-II)
AF076482	0.57	0.17	peptidoglycan recognition protein
AI835481	0.57	0.15	beta-1,3-glucuronyltransferase 3 (glucuronosyltransferase I)
AB033168	0.56	0.23	ZAP3 protein
U51167	0.56	0.03	isocitrate dehydrogenase 2 (NADP+), mitochondrial
AW124101	0.55	0.08	expressed sequence AA408278
X66091	0.54	0.08	*M. musculus* ASF mRNA
U11075	0.54	0.13	potassium inwardly-rectifying channel, subfamily J, member 4
D00472	0.51	0.15	cofilin 1, non-muscle
AJ006587	0.5	0.16	eukaryotic translation initiation factor 2, subunit 3, structural gene X-linked
AW048159	0.5	0.1	RIKEN cDNA 1200017E04 gene
AW212859	−0.53	0.12	axotrophin
AI843662	−0.53	0.2	stromal membrane-associated protein
AW046672	−0.53	0.08	DNA segment, Chr 11, ERATO Doi 603, expressed
L00993	−0.53	0.13	Sjogren syndrome antigen B
AW124044	−0.53	0.06	protein-L-isoaspartate (D-aspartate) *O*-methyltransferase 1
AW124329	−0.54	0.14	RIKEN cDNA 4921531G14 gene
AA839379	−0.55	0.14	RIKEN cDNA 2610002J02 gene
AI504338	−0.56	0.2	ESTs
AI844469	−0.56	0.13	RIKEN cDNA 0610012D09 gene
M34896	−0.56	0.14	ecotropic viral integration site 2
U83174	−0.57	0.22	gene trap ROSA 26, Philippe Soriano
AI853444	−0.59	0.22	RIKEN cDNA 2610042L04 gene
AA623587	−0.6	0.1	expressed sequence AA536743
U95498	−0.67	0.22	ALL1-fused gene from chromosome 1q

23 genes were down-regulated in the *gad* mice. These genes can be grouped according to their function (Table 1a) into RNA metabolism (3 up- and 0 down-regulated, 3/0), vesicle transport (3/0), proteins of the cell structure (3/1), channel proteins (4/0), calcium metabolism (2/0), growth factors (0/1), chaperones (1/0), signal transduction (11/2), membrane transport (4/0), transcription regulation (7/5), and others or unknown function (13/8). Nearly no gene of the immune-related proteins was found to be differentially regulated (2/0).

The criteria for moderate regulated genes were fulfilled by 134 genes with known or putative function and 12 ESTs without known function. A total of 103 of the genes were up-regulated, whereas 43 genes were down-regulated in the *gad* mice. These genes can be grouped according to their function (Table 1b) into RNA metabolism (4 up- and 0 down-regulated, 4/0), vesicle transport (4/0), proteins of the cell structure (5/1), defense (3/0), channel proteins (10/0), Lipid metabolisms (0/3), calcium metabolism (2/0), growth factors (0/2), chromatin structure (2/0), chaperones (1/1), signal transduction (21/4), membrane transport (5/0), transcription regulation (11/11), and others or unknown function (30/14).

Of the protein degradation pathway, six genes were down-regulated and another four genes were found to be up-regulated (Table 1a). Our first hypothesis that genes of the UCH gene family might compensate for the lack of UCH-L1 function was not confirmed. In contrast, UCH-L5 was found to be down-regulated.

At a first look, UCH-L1 was not differentially expressed. The reduction of the signal by the deletion of exons 7 and 8 is too weak for a change call of the Affymetrix software. However, the appropriate oligos show the absence of the corresponding RNA regions (data not shown).

An unsupervised, hierarchical cluster algorithm allowed us to cluster the five analyzed brains on the basis of their similarities measured over these 146 significant regulated genes from Table 1b (Fig. 1). In the dendrogram shown in Fig. 1 (left and top), the length and the subdivision of the branches display the relatedness of the brains (top) and the expression of the genes (left). Two distinct groups of brains (3 KO and 2 wt brains) and two groups of genes are shown.

4. Discussion

Ubiquitin has been implicated in numerous processes of the cell including cell-cycle control, receptor function,

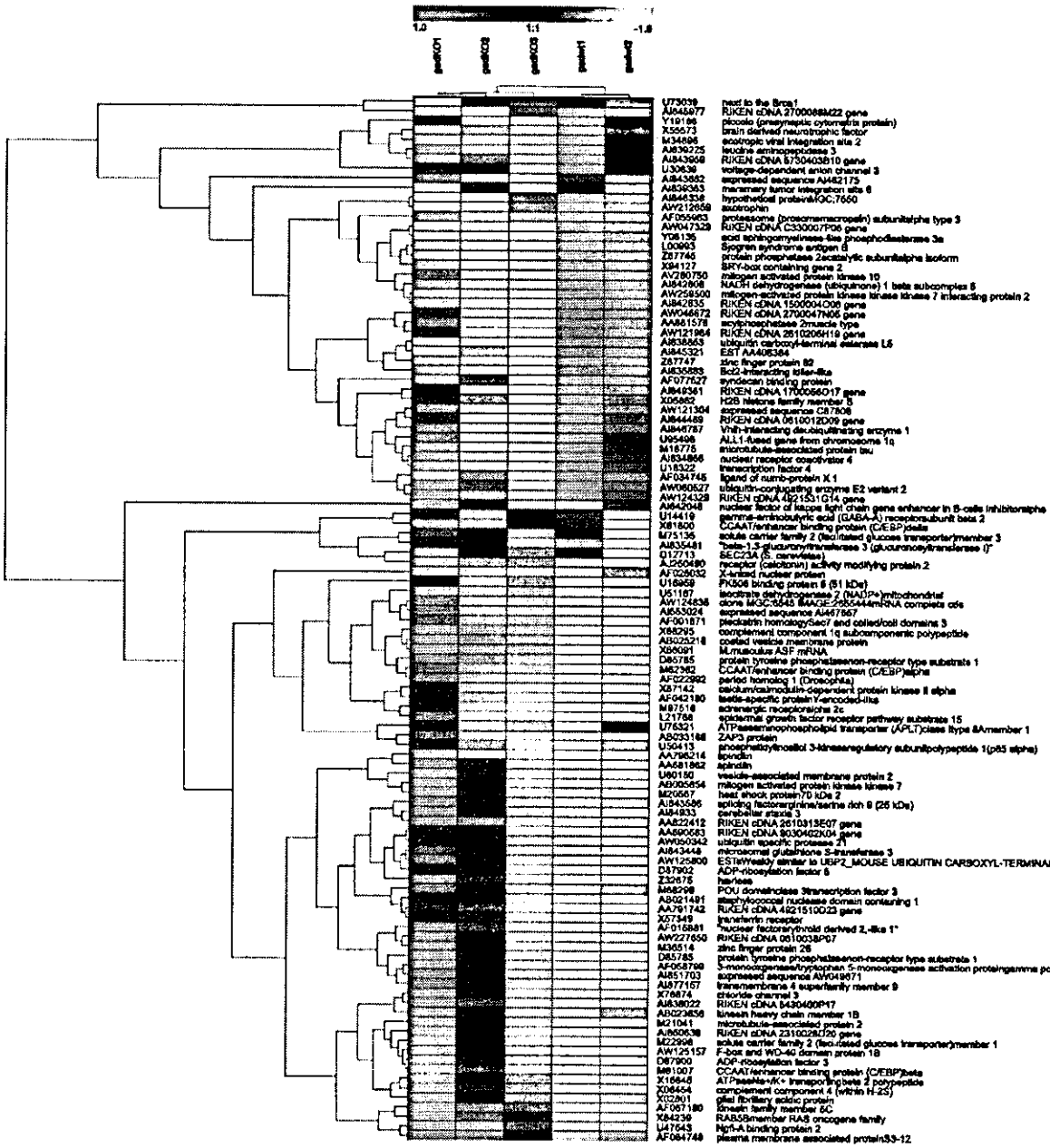

Fig. 1. Unsupervised two-dimensional cluster analysis of transcript ratios for the five mice brains (3 KO and 2 wt brains). There were 146 significant genes across the group. Each row represents a single gene and each column one brain. As shown in the colour bar, red indicates up-regulation, green down-regulation, black no change, and grey no data available.

signalling pathways, antigen presentation, degradation of proteins, and regulation of transcription. Analogous to these functions, alteration of the ubiquitin pathway will affect several of these pathways which may not be identifiable by single gene analysis. To investigate the complex network of gene regulation, we analyzed the expression pattern of 12,000 genes in 3-month-old male Uch-l1 deficient (*gad*) mice. This age was described to present the progressive phase of the disease [13]. The mutant mice used for this study showed sensory ataxia and motor paresis. Significant expression changes were found in more then 146 genes (Tables 1a and b). As expected, these genes are involved in several pathways of protein degradation, transcription regulation, vesicle and membrane transport, and signal transduction.

The gene most significantly down-regulated in the gad mice was Sox2 also known as SRY-box containing gene 2 (Signal log ratio −0.94, S.D. 0.14). Mutations of SOX2 cause anophthalmia in humans [9]. In mice, inactivation of Sox2 suggested a role in embryonal implantation [1]. SOX2

has been implicated in the regulation of Fgf4 expression [1]. In our experiments, we found no indication for a differential regulation of Fgf4, however, the inducible Fgf15 was down-regulated in *gad* mice (−0.65, S.D. 0.25) suggesting a role of Sox2 in Fgf15 expression and indicating a complex expression regulation mechanism of the Fgf gene family. Fgfs have been defined as regulators of the central nervous development and function (reviewed in Ref. [7]). However, the functional implication of a down-regulation of Fgf15 in mice has not been explored yet. Therefore, gad mice might suit as a model to study Fgf15 in more detail. Cofactors of Sox2 are totally unknown. One could speculate that transcription factors acting partially synergistic with Sox2 might be up-regulated in gad mice. In fact, we found several up-regulated transcription factors such as the eukaryotic translation initiation factor 2 (0.5, S.D. 0.16), the zinc finger protein 26 (1.19, S.D. 0.26), and CCAAT/enhancer binding protein (0.96, S.D. 0.23), respectively. Most convincingly, mRNAs of the alpha, beta, and delta subunits of the CCAAT/enhancer binding protein (C/EBP) were increased, respectively. Fig. 2 shows the central role of C/EBP. More than 20 adjusted genes can be implemented on a coherent biochemical network. For example, C/EBPs provide another link to the above-mentioned Fgf expression changes as a C/EBP site is an important regulatory element for FGF-binding protein activity [14]. Early changes of expression of C/EBP beta were also observed in other neurodegenerative diseases [21]. Most interestingly, only the inhibitory gamma and zeta subunits of C/EBP but not the positively functioning beta subunit have been found to be multi-ubiquinated and degraded by the proteasome [11]. We also found mRNA encoding the homeodomain interacting protein kinase 3 (HIPK3) to be up-regulated (1.26, S.D. 0.23). HIPK3 belongs to a family of co-repressors that potentiate the transcriptional activities of homeoproteins [16]. In gad mice, we found the homeobox gene containing transcription factor paired box gene 6 down-regulated (−0.44, S.D. 0.12). However, whether interaction of HIPK3 to the paired box gene 6 or other transcription factors as Sox2 is part of transcription activation has not been shown yet. Interestingly though, mutations in the paired box gene 6 causes eye diseases as mutations in Sox 2 [9]. How UCH-L1 is implicated in this process needs to be defined. For gad mice, however, abnormal eye development has not been described. It is likely that complete loss of function but no small alterations of the expression levels of these genes lead to the described developmental alterations. In gad mice, several other transduction pathways seem to be altered including the phosphatidylinositol 3 kinase (PI3K) pathway which is also linked to C/EBP. Specifically, the p85 alpha subunit of PI3K was found to be up-regulated (1.53; S.D. 0.92) (Fig. 2).

Besides the above-mentioned reduction of fgf15 mRNA, the brain-derived neurotrophic factor (BDNF) is also reduced in gad mice (−0.73, S.D. 0.23). BDNF has been reported to act on motor neurons [12] and to stimulate developmental neuro-muscular synapses [24]. Although BDNF reduction has not been reported yet in gad mice, one of us found significantly reduced NGF levels primarily in the spinal cord but not in the brain [29]. It has to be mentioned that spinal cord was not analyzed in our Chip analyses. However, in gad mice, decreased muscle weight has been observed with age which could be caused by the reduced BDNF and/or fgf15 levels, respectively. Although the function of another trophin, axotrophin, needs still to be explored, a reduction (−0.53, S.D. 0.12) of this factor implicates its significance in neuronal survival. In agreement with this hypothesis, Haendel and colleagues found neuronal degeneration in axotrophin-deficient mice (NCBI link NM_020575). In contrast, epidermal growth factor

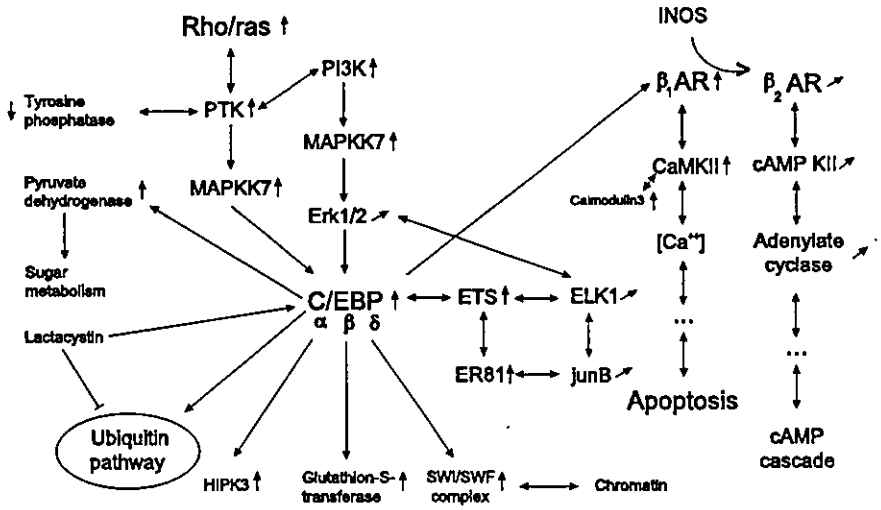

Fig. 2. C/EBP pathway demonstrating interactions of proteins which transcripts are differentially regulated in gad mice (up-regulated in six of six comparisons marked with ↑, upregulated genes in five or six of six comparisons are indicated with /, down-regulated in six of six comparisons are indicated with ↓).

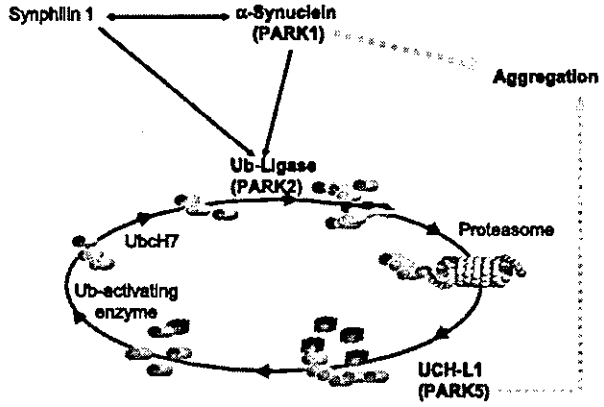

Fig. 3. Scheme of proteins altered in Parkinson's disease which place UCH-L1 as part of the altered protein degradation pathway and highlight the role of investigating Uch-l1-deficient (gad) mice by expression analysis.

receptor pathway substrate 15 was increased (0.83, S.D. 0.13) and might indicate a regulatory mechanism of gad mice trying to prevent neuronal degeneration.

Pathological features of gad mice are spheroid dystrophic axons dying back the dorsal root ganglia (DRG) progressing along the gracile tract of the spinal cord towards the parental neurons [15]. Immunohistochemically, almost all of the primary neurons and of the glial cells in DRG of gad mice revealed strong amyloid precursor protein (APP) staining [13]. The authors hypothesized abnormal expression of APP in gad mice as the cause of the pathological features. Although increased APP transcript in the brain has not been confirmed by our transcription analysis, amyloid beta (A4) precursor-like protein 2 was upregulated (0.59, S.D. 0.28). Our data also define an up-regulation of glial fibrillary acidic protein (GFAP) as the cause of the increased immunoreactivity of GFAP in astrocytes of gad mice [44].

We were in particular interested in genes involved in protein degradation. We hypothesized to find genes encoding proteins with UCH-L1 complementary functions compensatory up-regulated. Fig. 3 shows a simplified scheme of ubiquitin-altered protein degradation in PD and the task of UCH-L1. However, only the beta type 2 proteasome (prosome, macropain) subunit (0.66, S.D. 0.27) and the ubiquitin specific protease 21 (0.5, S.D. 0.09) were found to be increased. Interestingly, ubiquitin C-terminal hydrolase activity is associated with the 26S protease complex [8]. However, a direct interaction between UCH-L1 and macropain remains to be shown. Furthermore, Hsp70 protein 2 was increased (0.97, S.D. 0.31) likely due to decreased proteasomal degradation of proteins in gad mice, whereas Hsp70 protein 4 was down-regulated (− 0.56, S.D. 0.16). Ubiquitin carboxyl-terminal esterase L5 was also significantly decreased (− 0.59, S.D. 0.08).

In summary, the alteration of many pathways in gad mice offers an interesting mouse model which needs to be studied in more detail. The development of genome wide transcription profiles of mouse models in general will help to decipher the interaction and dependence of genes and gene products in their complexity of a living organism. Although it is not clear yet whether this complexity of biology in development, health and disease into their final details will be completely understood, a first step is being done to explore normal variation and disease processes at the RNA level using microarray chip analyses.

Acknowledgements

The authors thank D. Berg for the helpful discussions. This work was supported by a grant from the Federal Ministry of Education and Research (Fö. 01KS9602) and the Interdisciplinary Center of Clinical Research Tübingen (IZKF). Work of K.W. was supported by the grant for Research on Brain Science from the Ministry of Health, Labour and Welfare of Japan, Grants-in-Aid for Scientific Research from the Ministry of Education, Culture, Sports, Science and Technology of Japan, grants from the Organization for Pharmaceutical Safety and Research, and a grant from Japan Science and Technology Cooperation.

References

[1] A.A. Avilion, S.K. Nicolis, L.H. Pevny, L. Perez, N. Vivian, R. Lovell-Badge, Multipotent cell lineages in early mouse development depend on SOX2 function, Genes Dev. 17 (2003) 126–140.
[2] M.C. Bennett, J.F. Bishop, Y. Leng, P.B. Chock, T.N. Chase, M.M. Mouradian, Degradation of alpha-synuclein by proteasome, J. Biol. Chem. 274 (1999) 33855–33858.
[3] K.K.K. Chung, Y. Zhang, K.L. Lim, Y. Tanaka, H. Huang, J. Gao, et al., Parkin ubiquitinates the α-synuclein-interacting protein, synphilin-1: implications for Lewy-body formation in Parkinson disease, Nat. Med. 7 (2001) 1144–1150.
[4] A. Ciechanover, A.L. Schwartz, The ubiquitin–proteasome pathway: the complexity and myriad functions of proteins death, Proc. Natl. Acad. Sci. U. S. A. 95 (1998) 2727–2730.
[5] I.N. Day, L.J. Hinks, R.J. Thompson, The structure of the human gene encoding protein gene product 9.5 (PGP9.5), a neuron-specific ubiquitin C-terminal hydrolase, Biochem. J. 268 (1990) 521–524.
[6] M.C. DeRijk, C. Tzourio, M.M.B. Breteler, J.F. Dartigues, L. Amaducci, S. Lopez-Pousa, et al., Prevalence of parkinsonism and Parkinson's disease in Europe: the EUROPARKINSON collaborative study, J. Neurol. Neurosurg. Psychiatry 62 (1997) 10–15.
[7] R. Dono, Fibroblast growth factors as regulators of central nervous system development and function, Am. J. Physiol., Regul. Integr. Comp. Physiol. 284 (2003) R867–R881.
[8] E. Eytan, T. Armon, H. Heller, S. Beck, A. Hershko, Ubiquitin C-terminal hydrolase activity associated with the 26S protease complex, J. Biol. Chem. 268 (1993) 4668–4674.
[9] J. Fantes, N.K. Ragge, S.A. Lynch, N.I. McGill, J.R. Collin, P.N. Howard-Peebles, C. Hayward, A.J. Vivian, K. Williamson, V. Van Heyningen, D.R. Fitz Patrick, Mutations in SOX2 cause anophthalmia, Nat. Genet. 33 (2003) 461–463.
[10] L.I. Golbe, G. Di Iorio, G. Sanges, A.M. Lazzarini, S. La Salsa, V. Bonavita, et al., Clinical genetic analysis of Parkinson's disease in the Contursi kindred, Ann. Neurol. 40 (1996) 767–775.
[11] T. Hattori, N. Ohoka, Y. Inoue, H. Hayashi, K. Onozaki, C/EBP family transcription factors are degraded by the proteasome but stabilized by forming dimmer, Oncogene 22 (2003) 1273–1280.

[12] C.E. Henderson, W. Camu, C. Mettling, A. Gouin, K. Poulsen, M. Karihaloo, J. Rullamas, T. Evans, S.B. McMahon, M.P. Armanini, L. Berkemeier, H.S. Phillips, A. Rosenthal, Neurotrophins promote motor neuron survival and are present in embryonic limb bud, Nature 364 (1993) 266–270.
[13] N. Ichihara, J. Wu, D.H. Chui, K. Yamazaki, T. Wakabayashi, T. Kikuchi, Axonal degeneration promotes abnormal accumulation of amyloid beta-protein in ascending gracile tract of gracile axonal dystrophy (GAD) mouse, Brain Res. 695 (1995) 173–178.
[14] B.L. Kagan, R.T. Henke, R. Cabal-Manzano, G.E. Stoica, Q. Nguyen, A. Wellstein, A.T. Riegel, Complex regulation of the fibroblast growth factor-binding protein in MDA-MB-468 breast cancer cells by CCAAT/Enhancer-binding protein beta, Cancer Res. 63 (2003) 1696–1705.
[15] T. Kikuchi, M. Mukoyama, K. Yamazaki, H. Moriya, Axonal degeneration of ascending sensory neurons in gracile axonal dystrophy mutant mouse, Acta Neuropathol. 80 (1990) 145–151.
[16] Y.H. Kim, C.Y. Choi, S.-J. Lee, M.A. Conti, Y. Kim, Homeodomain-interacting protein kinases, a novel family of co-repressors for homeodomain transcription factors, J. Biol. Chem. 273 (1998) 25875–25879.
[17] T. Kitada, S. Asakawa, N. Hattori, H. Matsumine, Y. Yamamura, S. Minoshima, et al., Mutations in the parkin gene cause autosomal recessive juvenile parkinsonism, Nature (London) 392 (1998) 605–608.
[18] R. Kruger, W. Kuhn, T. Muller, D. Woitalla, M. Graeber, S. Kosel, H. Przuntek, J.T. Epplen, L. Schols, O. Riess, Ala30Pro mutation in the gene encoding alpha-synuclein in Parkinson's disease, Nat. Genet. 18 (1998) 106–108.
[19] R. Kruger, O. Eberhardt, O. Riess, J.B. Schulz, Parkinson's disease: one biochemical pathway to fit all genes? Trends Mol. Med. 8 (2002) 236–240.
[20] E. Leroy, R. Boyer, G. Auburger, B. Leube, G. Ulm, E. Mezey, G. Brownstein, M.J. Brownstein, S. Jonnalagada, T. Chernova, et al., The ubiquitin pathway in Parkinson's disease, Nature 395 (1998) 451–452.
[21] A.P. Lieberman, G. Harmison, A.D. Strand, J.M. Olson, K.H. Fischbeck, Altered transcriptional regulation in cells expressing the expanded polyglutamine androgen receptor, Hum. Mol. Genet. 11 (2002) 1967–1976.
[22] G. Liu, A.E. Loraine, R. Shigeta, M. Cline, J. Cheng, V. Valmeekam, S. Sun, D. Kulp, M.A. Siani-Rose, NetAffx: affymetrix probesets and annotations, Nucleic Acids Res. 31 (2003) 82–86.
[23] Y. Liu, L. Fallon, H.A. Lashuel, Z. Liu , P.T. Lansbury Jr., The UCH-L1 gene encodes two opposing enzymatic activities that affect alpha-synuclein degradation and Parkinson's disease susceptibility, Cell 111 (2002) 209–218.
[24] A.M. Lohof, Y. Ip, M. Poo, Potentiation of developing neuromuscular synapses by the neurotrophins NT-3 and BDNF, Nature 363 (1993) 350–353.
[25] J. Lowe, H. McDermott, M. Landon, R.J. Mayer, K.D. Wilkinson, Ubiquitin carboxyl-terminal hydrolase (PGP 9.5) is selectively present in ubiquitinated inclusion bodies characteristic of human neurodegenerative diseases, J. Pathol. 161 (1990) 153–160.
[26] C.B. Lücking, A. Dürr, V. Bonifati, J. Vaugham, G. De Michele, T. Gasser, et al., Association between early-onset Parkinson's disease and mutations in the parkin gene, N. Engl. J. Med. 342 (2000) 1560–1567.
[27] D.M. Maraganore, M.J. Farrer, J.A. Hardy, S.J. Lincoln, S.K. McDonnell, W.A. Rocca, Case-control study of the ubiquitin carboxy-terminal hydrolase L1 gene in Parkinson's disease, Neurology 53 (1999) 1858–1860.
[28] F.P. Marx, C. Holzmann, K.M. Strauss, L. Li, O. Eberhard, M. Cookson, et al., Identification and functional characterization of a novel R621C mutation in the synphilin-1 gene in Parkinson's disease, Hum. Mol. Genet. 12 (2003) 1223–1231.
[29] K. Matsui, S. Furukawa, J.-G. Suh, K. Wada, Developmental changes of nerve growth factor levels in the gracile axonal dystrophy mouse, Neurosci. Lett. 177 (1994) 116–118.
[30] K.S. McNaught, L.M. Bjorklund, R. Belizaire, O. Isacson, P. Jenner, C.W. Olanow, Proteasome inhibition causes nigral degeneration with inclusion bodies in rats, NeuroReport 13 (2002) 1437–14411.
[31] D.J. Nicholl, J.R. Vaughan, N.L. Khan, S.L. Ho, D.E.W. Aldous, S. Lincoln, et al., Two large British kindreds with familial Parkinson's disease: a clinico-pathological and genetic study, Brain 125 (2002) 44–57.
[32] K. Nishikawa, H. Li, R. Kawamura, H. Osaka, Y.L. Wang, Y. Hara, et al., Alterations of structure and hydrolase activity of parkinsonism-associated human ubiquitin carboxyl-terminal hydrolase L1 variants, Biochem. Biophys. Res. Commun. 304 (2003) 176–183.
[33] H. Osaka, Y.L. Wang, K. Takada, S. Takizawa, R. Setsuie, H. Li, Y. Sato, et al., Ubiquitin carboxy-terminal hydrolase L1 binds to and stabilizes monoubiquitin in neuron, Hum. Mol. Genet. 12 (2003) 1945–1958.
[34] E. Ozkaynak, D. Finley, M.J. Solomon, A. Varshavsky, The yeast ubiquitin genes: a family of natural gene fusions, EMBO J. 6 (1987) 1429–1439.
[35] P. Piccini, D.J. Burn, R. Ceravolo, D. Maraganore, D.J. Brooks, The role of inheritance in sporadic Parkinson's disease: evidence from a longitudinal study of dopaminergic function in twins, Ann. Neurol. 45 (1999) 577–582.
[36] M.H. Polymeropoulos, C. Lavedan, E. Leroy, S.E. Ide, A. Dehejia, A. Dutra, B. Pike, H. Root, J. Rubenstein, R. Boyer, E.S. Stenroos, S. Chandrasekharappa, A. Athanassiadou, T. Papapetropoulos, W.G. Johnson, A.M. Lazzarini, R.C. Duvoisin, G. Di Iorio, L.I. Golbe, R.L. Nussbaum, Mutation in the alpha-synuclein gene identified in families with Parkinson's disease, Science 276 (1997) 2045–2047.
[37] K. Saigoh, Y.L. Wang, J.G. Suh, T. Yamanishi, Y. Sakai, H. Kiyosawa, T. Harada, N. Ichihara, S. Wakana, T. Kikuchi, K. Wada, Intragenic deletion in the gene encoding ubiquitin carboxy-terminal hydrolase in gad mice, Nat. Genet. 23 (1999) 47–51.
[38] H. Shimura, N. Hattori, S.-I. Kubo, Y. Mizuno, S. Asakawa, S. Minoshima, et al., Familial Parkinson disease gene product, parkin, is a ubiquitin-protein ligase, Nat. Genet. 25 (2000) 302–305.
[39] A. Sturn, J. Quackenbush, Z. Trajanoski, Genesis: cluster analysis of microarray data, Bioinformatics 18 (2002) 207–208.
[40] G.K. Tofaris, R. Layfield, M.G. Spillantini, Alpha-synuclein metabolism and aggregation is linked to ubiquitin-independent degradation by the proteasome, FEBS Lett. 509 (2001) 22–26.
[41] K.D. Wilkinson, K.M. Lee, S. Deshpande, P. Duerksen-Hughes, J.M. Boss, J. Pohl, The neuron-specific protein PGP 9.5 is a ubiquitin carboxyl-terminal hydrolase, Science 246 (1989) 670–673.
[42] P. Wintermeyer, R. Krüger, W. Kuhn, T. Müller, D. Woitalla, D. Berg, et al., Mutation analysis and association studies of the UCHL1 gene in German Parkinson's disease patients, NeuroReport 11 (2000) 2079–2082.
[43] Z.K. Wszolek, B. Pfeiffer, J.R. Fulgham, J.E. Parisi, B.M. Thompson, R.J. Uitti, et al., Western Nebraska family (family-D) with autosomal dominant parkinsonism, Neurology 45 (1995) 502–505.
[44] K. Yamazaki, H. Moriya, N. Ichihara, H. Mitsushio, S. Inagaki, T. Kikuchi, Substance P-immunoreactive astrocytes in gracile sensory nervous tract of spinal cord in gracile axonal dystrophy mutant mouse, Mol. Chem. Neuropathol. 20 (1993) 1–20.

Available online at www.sciencedirect.com

SCIENCE DIRECT

Brain Research 1019 (2004) 1–9

BRAIN RESEARCH

www.elsevier.com/locate/brainres

Research report

Accumulation of β- and γ-synucleins in the ubiquitin carboxyl-terminal hydrolase L1-deficient *gad* mouse

Yu-Lai Wang[a], Ayako Takeda[a], Hitoshi Osaka[a,b], Yoko Hara[a], Akiko Furuta[a], Rieko Setsuie[a,c], Ying-Jie Sun[a], Jungkee Kwon[a,d], Yae Sato[a,c], Mikako Sakurai[a,c], Mami Noda[c], Yasuhiro Yoshikawa[d], Keiji Wada[a,*]

[a] *Department of Degenerative Neurological Diseases, National Institute of Neuroscience, National Center of Neurology and Psychiatry, Kodaira, Tokyo 187-8502, Japan*

[b] *Information and Cellular Function, PRESTO, Japan Science and Technology Agency (JST), Kawaguchi, Saitama 332-0012, Japan*

[c] *Laboratory of Pathophysiology, Graduate School of Pharmaceutical Sciences, Kyushu University, Higashi, Fukuoka, 812-8582, Japan*

[d] *Department of Biomedical Science, Graduate School of Agricultural and Life Sciences, University of Tokyo, 1-1-1 Yayoi, Bunkyo, Tokyo, 113-8657, Japan*

Accepted 11 May 2004

Abstract

The synuclein family includes three isoforms, termed α, β and γ. α-Synuclein accumulates in various pathological lesions resulting from neurodegenerative disorders including Parkinson's disease (PD), dementia with Lewy bodies (DLB) and multiple system atrophy. However, neither β- nor γ-synuclein has been detected in Lewy bodies, and thus it is unclear whether these isoforms contribute to neurological pathology. In the present study, we used immunohistochemistry to demonstrate accelerated accumulation of β- and γ-synucleins in axonal spheroids in gracile axonal dystrophy (*gad*) mice, which do not express ubiquitin carboxyl-terminal hydrolase L1 (UCH-L1). γ-Synuclein immunoreactivity in the spheroids appeared in the gracile nucleus at 3 weeks of age and was maintained until 32 weeks. β-Synuclein immunoreactivity appeared in spheroids around 12 weeks of age. In contrast, α-synuclein immunoreactivity was barely detectable in spheroids. Immunoreactivity for synaptophysin and ubiquitin were either faint or undetectable in spheroids. Given that UCH-L1 deficiency results in axonal degeneration and spheroid formation, our findings suggest that β- and γ-synuclein participate in the pathogenesis of axonal swelling in *gad* mice.

Theme: Disorders of the nervous system
Topic: Degenerative disease: other

Keywords: Synuclein; Spheroid; UCH-L1; Ubiquitin

1. Introduction

The synucleins are a family of small cytosolic proteins that are expressed abundantly in the nervous system. Their contribution to neurophysiological function, however, is poorly understood. The mouse synuclein family consists of three members, α-synuclein (α-syn), β-synuclein (β-syn) and γ-synuclein (γ-syn), which range from 123 to 140 residues in length, exhibit 48–58% amino acid sequence identity and share similar domain organization (Fig. 1). Immunohistochemistry in the normal brain shows that α- and β-syn are concentrated at nerve terminals with little staining of somata and dendrites. Ultrastructural studies show that these isoforms localize to nerve terminals in close proximity to synaptic vesicles [18]. In contrast, γ-syn is present throughout nerve cells and is most abundant in the peripheral nervous system [5,18].

The synuclein family has been implicated in neurodegenerative diseases. Two point mutations (A53T, A30P) in the gene encoding α-synuclein (*SNCA*) have been detected in two distinct Parkinson's disease (PD) sibships with autosomal dominant inheritance [17,26], and a heritable

* Corresponding author. Tel.: +81-42-346-1715; fax: +81-42-346-1745.
E-mail address: wada@ncnp.go.jp (K. Wada).

0006-8993/$ - see front matter © 2004 Elsevier B.V. All rights reserved.
doi:10.1016/j.brainres.2004.05.023

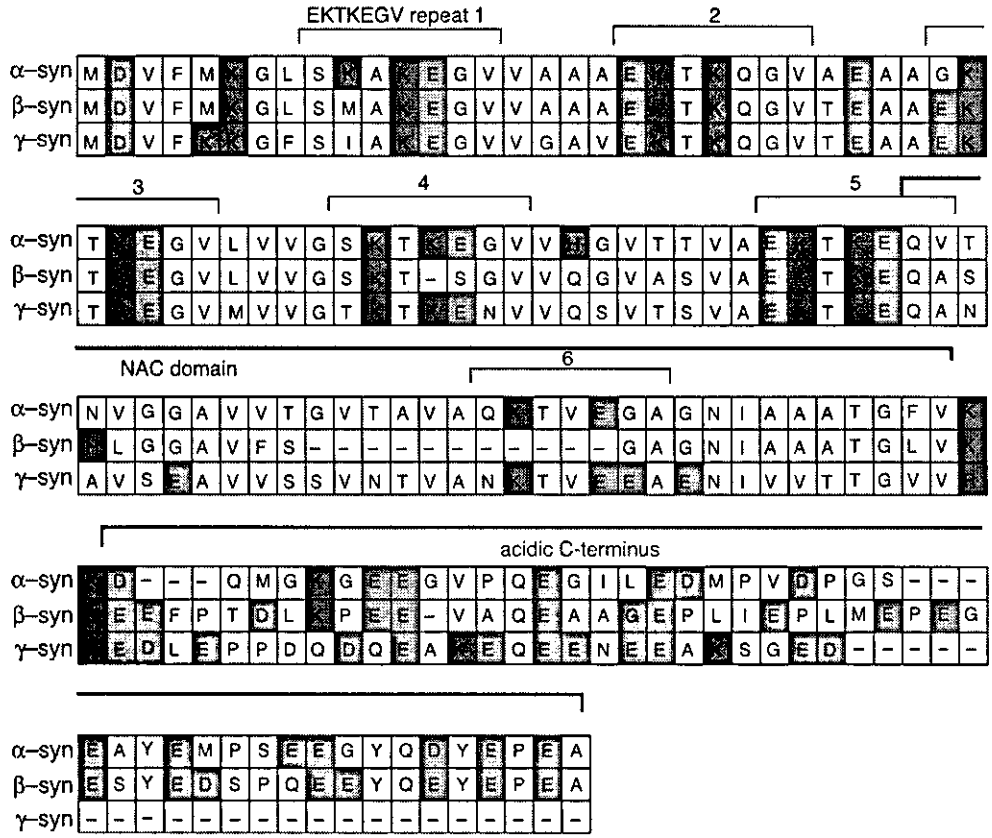

Fig. 1. Comparison of amino acid sequences from mouse α-, β- and γ-synuclein. The N-terminal region contains six imperfect repeats of the consensus EKTKEGV and the C-terminal region is negatively charged. A part of the hydrophobic NAC (non-amyloid component of amyloid plaque) domain is deleted in β-syn. Basic and acidic residues are shown in blue and red, respectively. Sequence accession numbers: mouse α-syn, NP-033247; mouse β-syn, NP-291088; mouse γ-syn, NP-035560.

genomic triplication of *SNCA* has been described within two distinct families [6,33]. Also, α-synuclein protein is a primary component of Lewy bodies (intracellular inclusions) and accumulates in abnormal neurites that contain ubiquitin, synaptophysin and neurofilaments [9,36,37]. β-Syn and γ-syn, which is also known as breast cancer-specific gene 1 (*BCSG1*), are overexpressed in neurodegenerative diseases such as PD and dementia with Lewy bodies (DLB) [5,7]. Unlike α- and β-syn, γ-syn is distributed throughout the cytoplasm of neurons where it influences the integration of neurofilament networks [4].

Ubiquitin carboxyl-terminal hydrolase L1 (UCH-L1) has been found throughout the brain and testis/ovary and has been considered as plays an important role in the labeling of abnormal proteins in the ubiquitin-proteasome system [15,38]. The gracile axonal dystrophy (*gad*) mouse is an autosomal recessive spontaneous mutant that was identified in 1984 [42]. It is the first mammalian neurological model with a defect in the ubiquitin-proteasome system [28]. These mice carry an intragenic deletion of the UCH-L1 gene (*Uchl1*) and do not express UCH-L1, making them comparable to a *Uchl1* null mutant [24,28]. The *gad* mouse exhibits severe sensory ataxia at an early stage, followed by motor paresis at a later stage [14,42]. In the central nervous system of *gad* mice, axonal degeneration begins from the distal ends of primary ascending axons in the dorsal root ganglia (DRG) [21,22]. Spheroid formation with the dying-back type of axonal degeneration is first observed in the gracile and dorsal spinocerebellar tracts [14,21,42]. In the most rostral portion of the gracile fascicles, spheroids are observed around 12 weeks of age and their formation progresses gradually to the terminal stage after 20 weeks of age [22]. At a later stage, axonal degeneration and spheroid formation are observed in the upper tracts of DRG neurons as well as in motor neurons [22]. Although the *gad* mutation is known to be caused by a deficiency in UCH-L1, the mechanism of spheroid formation is not well understood. Dystrophic axons or axonal spheroids have been observed in the brains of patients with infantile neuroaxonal dystrophy [1], in the globus pallidus in Hallervorden-Spatz disease [10], and in the gracile and cuneate nuclei in human vitamin-E deficiency [29]. Furthermore, spheroids are often observed in the medulla and spinal cords of aged mammals. In normal mice, the number of spheroids increases with age in the gracile nucleus [43].

Components of the spheroids of *gad* mice include amyloid-β protein, mitochondria, neurofilaments and synaptic complexes [12,22]. Ubiquitin and amyloid-β protein

also accumulate outside spheroids along the sensory and motor nervous systems [12,40]. We previously observed dot-like deposits of ubiquitin immunoreactivity throughout the gracile nucleus [40]. These data led us to suggest that the absence of functional UCH-L1 may affect the hydrolysis of unknown substrates, which could result in the formation of protein aggregates. α-Syn accumulation has been detected in spheroids resulting from type 1 iron accumulation in the brain (NBIA 1), a rare neurodegenerative disorder characterized by axonal spheroids and Lewy body-like intraneuronal inclusions [8]. Moreover, β-syn and γ-syn immunoreactivity were detected in spheroids but not in Lewy body-like inclusions [8]. In PD and DLB, axonal spheroid-like lesions were identified in the molecular layer of the dentate gyrus along with the accumulation of γ-syn, but not of α- or β-syn [7].

In the present study, we investigated the accumulation of α-syn, β-syn and γ-syn in the *gad* mouse using isoform-specific antibodies. Unexpectedly, we did not detect α-syn in spheroids, although β-syn and γ-syn accumulated in these structures beginning at an early stage of pathology. These results demonstrate that the *gad* mouse constitutes a useful model for investigating the role of synucleins in neurodegeneration.

2. Materials and methods

2.1. Animals

All mice were maintained and propagated at our institute. Adult homozygous *gad/gad* and wild-type (+/+) mice were obtained by mating heterozygous males with heterozygous females. All mouse experiments were performed in accordance with our institution's regulations for animal care and with the approval of the Animal Investigation Committee of the National Institute of Neuroscience, National Center of Neurology and Psychiatry. Each experimental group consisted of three male mice of the same phenotype, and experiments were conducted at 3 weeks (initial stage), 12 weeks (progressive stage), 17 and 20 weeks (critical stage), and 32 weeks (terminal stage) after birth [44].

2.2. Histochemistry

Mice were anesthetized and perfused with 0.9% NaCl followed by ice-cold 4% paraformaldehyde in phosphate-buffered saline (PBS, pH 7.4). Brains and spinal cords were then collected and postfixed in 4% paraformaldehyde overnight at 4 °C. The medulla oblongata and the upper cervical cord were examined. To ensure near complete concordance in the anatomical level of each sample, we followed the Atlas of the Mouse Brain and Spinal Cord [32]. Coronal sections were made at the level of the gracile nucleus (level 535) and of the cervical (C3) spinal cord segments. The samples were embedded in paraffin and sectioned (4 μm) for immunostaining and light microscopy. All sections from mice of the same age group were processed in parallel for each marker. Some sections were stained with hematoxylin–eosin (HE) and Klüver-Barrera for examination by conventional pathological methods. Quantification using stereological techniques was performed by counting eosinophilic spheroids at the medulla and upper cervical levels in at least three sections per sample by two blind observers. We then calculated the average number of spheroids per section. Spheroids were counted using the 200 × lens of a Zeiss Axioplan microscope. Under this magnification, eosinophilic spheroids are clearly viewed.

For immunohistochemistry, serial sections were deparaffinized in xylene and graded ethanol, washed in distilled water, and then treated with 0.3% H_2O_2 in methanol for 30 min to quench endogenous peroxidase activity. For the enhancement of α-syn immunostaining, sections were pretreated with 99% formic acid for 5 min or autoclaved at 121 °C for 10 min [35,36]. The sections were washed three times for 5 min in PBS, and then nonspecific binding sites were blocked by incubation in 10% normal serum obtained from the species in which the secondary antibody was generated. After a brief rinse with PBS, sections were incubated overnight at 4 °C with primary antibodies. Primary and secondary antibodies were diluted in DAKO Antibody Diluent (Dako, CA). The following antibodies were used at the final dilutions indicated: monoclonal α-syn antibody (1:100; BD Transduction Laboratories, CA), polyclonal β-syn antibody (1:200; Affinity Research Products), monoclonal synaptophysin antibody (1:50; Dako) and polyclonal ubiquitin antibody (1:400; Chemicon, Temecula). Polyclonal γ-syn antibody (see below) was diluted 1:100.

Subsequent antibody detection was carried out using anti-rabbit or anti-mouse IgG from the VECTASTAIN Elite ABC kit (Vector Labs, Burlingame, CA). Briefly, after washing, sections were sequentially incubated with biotinylated secondary antibodies for 1 h followed by avidin–biotin complex (diluted 1:200) for 1 h. Bound antibody complexes were visualized using 3,3′-diaminobenzidine tetrachloride as a peroxidase substrate. Sections were then lightly counterstained with hematoxylin. For the blocking experiments, anti-γ-syn was initially incubated with recombinant γ-syn for 4 h at 4 °C and the staining procedure was then performed as described above. The sections from different groups were immunostained and treated at the same time. For controls, the primary antibody was replaced with normal rabbit serum or was omitted (these controls always yielded negative staining).

2.3. Preparation of γ-syn antibody and antibody purification

γ-Syn cDNA was cloned from mouse brain mRNA using PCR with a primer set designed using the γ-syn nucleotide

sequence in GenBank (AF017255; sense primer, 5′-ACATGCATGCGACGTCTTCAAGAAAGGCTTC-3′; antisense primer, 5′-CCCAAGCTTGTCTTCTCCACTCTTGGC-3′). The γ-syn cDNA was cloned into the expression vector pEQ-30 (Qiagen, Germany), yielding a recombinant plasmid used to express histidine-tagged γ-syn (6-His-γ-syn) in *E. coli*. Recombinant 6-His-γ-syn was prepared as previously described [23] and used to generate a polyclonal antiserum in rabbits (Takara, Japan). The polyclonal antibodies were purified by affinity chromatography according to the manufacturer's instructions.

2.4. Specificities of synuclein antibodies

Purified recombinant α-syn (BD Transduction Laboratories), β-syn (Alpha Diagnostic International, TX) and γ-syn were diluted and subjected to electrophoresis through SDS-polyacrylamide gels (15% acrylamide) at 200, 100, 50, 25 and 12.5 ng per lane for each protein. The proteins were electrophoretically transferred to PVDF membranes (Bio-Rad, CA) as previously reported [23]. For immunochemical detection of the proteins, the membranes were first blocked in Tris-buffered saline containing 0.1% (w/v) Tween 20 (TTBS) and 3% BSA overnight at 4 °C and then incubated for 12 h with anti-α-syn (1:1000) or with anti-β- or anti-γ-syn (1:500). Antibodies were diluted in DAKO Antibody Diluent. The membranes were washed with TTBS and then incubated with horseradish peroxidase (HRP)-conjugated goat anti-rabbit or anti-mouse IgG (1:10,000; Pierce, IL) for 1 h. Proteins were detected using the SuperSignal chemiluminescence system (Pierce).

3. Results

3.1. Histopathological analysis of the gracile nucleus by HE staining

Oval or round spheroids were visualized by HE staining of axonal sections from wild-type mice at 20 weeks of age. However, fewer than five spheroids per section were detected. In contrast, gracile nuclei of *gad* mice exhibited both axonal dystrophy and spheroids as early as 3 weeks of age (Fig. 2A), in agreement with a previous report [44]. The number of spheroids increased with age, and the HE staining intensity of spheroids was relatively high until 20 weeks of age (Fig. 2B,C) but was very faint at 32 weeks (Fig. 2D). The size and appearance of the spheroids detected in *gad* mice varied with age. Irregularly shaped spheroids were observed from 12 to 20 weeks, whereas other spheroids stained diffusely or granularly as observed in wild-type mice (Fig. 2E). Some spheroids displayed an intense eosinophilic core, vacuoles or thin clefts (Fig. 2B).

We manually counted the total number of spheroids in the dorsal columns and dorsal nuclei of the medulla and upper cervical spinal cord using stereological techniques. Spheroids were detected in *gad* mice at all ages examined (Fig. 2F). The number of spheroids increased with age until 20 weeks (mean ± S.D.; $n = 8 \sim 13$): 3 weeks, 3.2 ± 0.8; 12 weeks, 12.1 ± 3.4; 20 weeks, 16.3 ± 3.9. At 32 weeks, however, the number of spheroids decreased (7.8 ± 2.2), as did their size (data not shown). These observations most likely reflect the severity of degeneration following the progression of the dying-back type of axonal dystrophy [14,44] to the lower spinal cord. In comparison, only a very

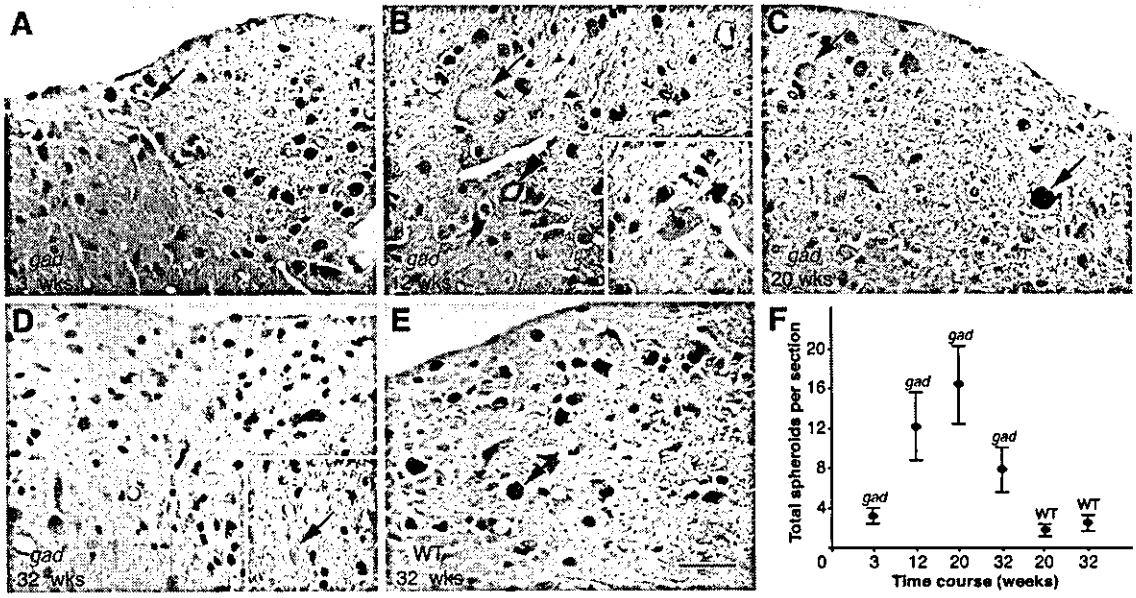

Fig. 2. Hematoxylin–eosin staining of eosinophilic spheroids (arrows) in (A–D) gad sections of the gracile nucleus of the medulla oblongata at 3, 12, 20 and 32 weeks of age, respectively, and in (E) a wild-type section at 32 weeks. An arrowhead indicates a vacuolar spheroid body, and a white arrow indicates a spheroid with an intense eosinophilic core (inset in B). (F) A quantitative study of spheroid number over time in gad and WT mice. Values are the mean ± S.D. ($n = 8 \sim 13$). Bar = 50 μm.

small number of spheroids were found in wild-type mice (1.8±0.6 at 20 weeks, 2.5 ± 0.8 at 32 weeks; $n=9$; Fig. 2F).

3.2. Spheroids of gad mice accumulate β-syn and γ-syn but lack α-syn

We tested the specificity of the synuclein antibodies using purified recombinant synuclein isoforms. Polyclonal anti-γ-syn recognized purified recombinant γ-syn but did not cross-react with recombinant α-syn or β-syn in western blots (Fig. 3C). This antibody was also useful for immunohistochemical detection of γ-syn in spheroids in the gracile nucleus (Fig. 4A–D). No staining was observed when polyclonal anti-γ-syn was pre-absorbed with recombinant γ-syn (1:20 antibody/protein molar ratio; data not shown), thereby demonstrating the specificity of the staining. Under the same conditions, controls without anti-γ-syn showed no immunoreactivity (data not shown). An assay of specificity was also performed using the commercial antibodies against α-syn and β-syn, and similar results were obtained for both antibodies (Fig. 3A,B).

We then utilized all three isoform-specific antibodies to characterize the pathology of axonal degeneration in the *gad* mouse. Immunoreactivity to γ-syn was robust during postnatal weeks 3 ~ 20 but was weak at week 32 (Table 1). At 3 weeks of age, the spheroids detected by anti-γ-syn were more clearly recognized than those detected by HE staining. γ-Syn-immunoreactive spheroids varied in appearance as shown by HE staining (Fig. 2A–D), and oval or round spheroids were often diffusely or granularly immunostained

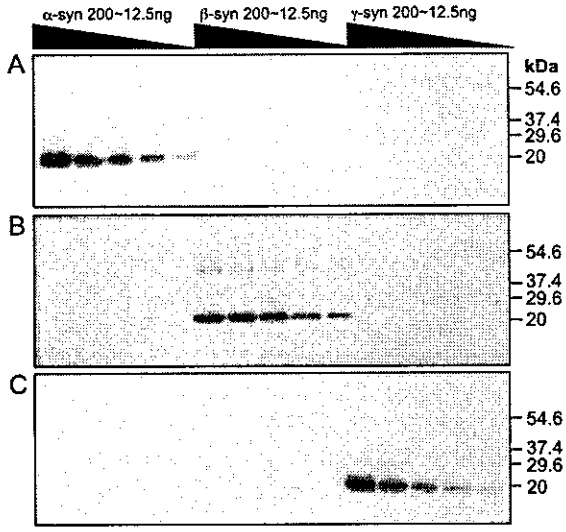

Fig. 3. Specificity of synuclein antibodies. Western blots show the specificity and reactivity of anti-α-syn, anti-β-syn and anti-γ-syn with varying amounts (12.5 ~ 200 ng) of all three recombinant synucleins. Three identical SDS-polyacrylamide gels were transferred to membranes under identical conditions, and each membrane was then probed separately with one of the synuclein antibodies. (A) α-syn antibody. (B) β-syn antibody. (C) γ-syn antibody. None of the antibodies exhibited significant cross-reactivity. A dimer formation (~ 50 kDa) was seen in the β-syn blot (B). Molecular weight markers (in kDa) are shown to the right.

by anti-γ-syn (Fig. 4A–C). Numerous dystrophic axons also displayed γ-syn immunoreactivity. γ-Syn immunoreactivity was absent both in spheroids and dystrophic axons when anti-γ-syn was pre-incubated with excess purified γ-syn (data not shown). In contrast to γ-syn immunoreactivity, spheroids started to exhibit faint and sporadic β-syn immunostaining from 12 weeks of age, with the intensity increasing through 32 weeks (Fig. 4E,F and Table 1). At 32 weeks, relatively intense β-syn staining was observed in spheroids and dystrophic axons (Fig. 4G); however, there were fewer immunopositive spheroids than were seen by γ-syn staining (at 20 weeks; Fig. 4C). Coarse granules around neurons were also immunostained by anti-β-syn (Fig. 4G). Very little α-syn immunoreactivity was observed in spheroids even after enhancement with formic acid or by autoclaving (Fig. 4I). These pretreatments also failed to show α-syn immunoreactivity in axons (Fig. 4I).

In wild-type mice, spheroids were immunopositive for γ-syn (Fig. 4D) and β-syn (a relatively weak punctate pattern in the center of spheroids; Fig. 4H). However, no α-syn immunoreactivity was detected (Fig. 4J, arrows). Also, ubiquitin-positive immunostaining, which did not appear until 20 weeks, was seen in spheroids and as dots that did not correspond to spheroids (data not shown). In *gad* mice, ubiquitin-immunoreactive dots appeared from 12 weeks of age as previously demonstrated [40] and spheroids were not immunoreactive for ubiquitin (Fig. 4K). Ubiquitin staining in general was more intense in the wild-type tissue (Fig. 4L) than in *gad* tissue (Fig. 4K). For synaptophysin, the limited number of spheroids were immunopositive in both wild-type and *gad* mice at 20 weeks of age, with a diffuse or spotty staining in the center of the spheroids (Fig. 4M,O). The *gad* mouse appears to show higher synaptophysin expression than wild-type mice (Fig. 4M,O). At 32 weeks, *gad* mice displayed a punctate distribution pattern of synaptophysin along synapses or surrounding cell bodies with a few densely stained spheroids (Fig. 4N, arrow). In contrast, wild-type mice displayed an expression pattern that was enriched in the spheroids at 32 weeks of age (Fig. 4P, arrow). Furthermore, *gad* mice exhibited dot-like immunostaining for ubiquitin (Fig. 4L, arrowheads), β-syn (Fig. 4G) and γ-syn (Fig. 4C).

4. Discussion

Previous studies of *gad* mice showed axonal degeneration and spheroid-formation (axonal dystrophy) in the gracile tract during the initial stage of neuropathology [14,22,44]. During the critical stage from 17 to 20 weeks of age, the pathological changes extend to the spinocerebellar tract and spinal trigeminal nucleus. During the terminal stage (beyond 32 weeks), these changes extend to the corticospinal tract, cuneate tract, spinal trigeminal tract and thalamus [44]. Although synucleins have been implicated in the pathology of various neurodegenerative disorders, the

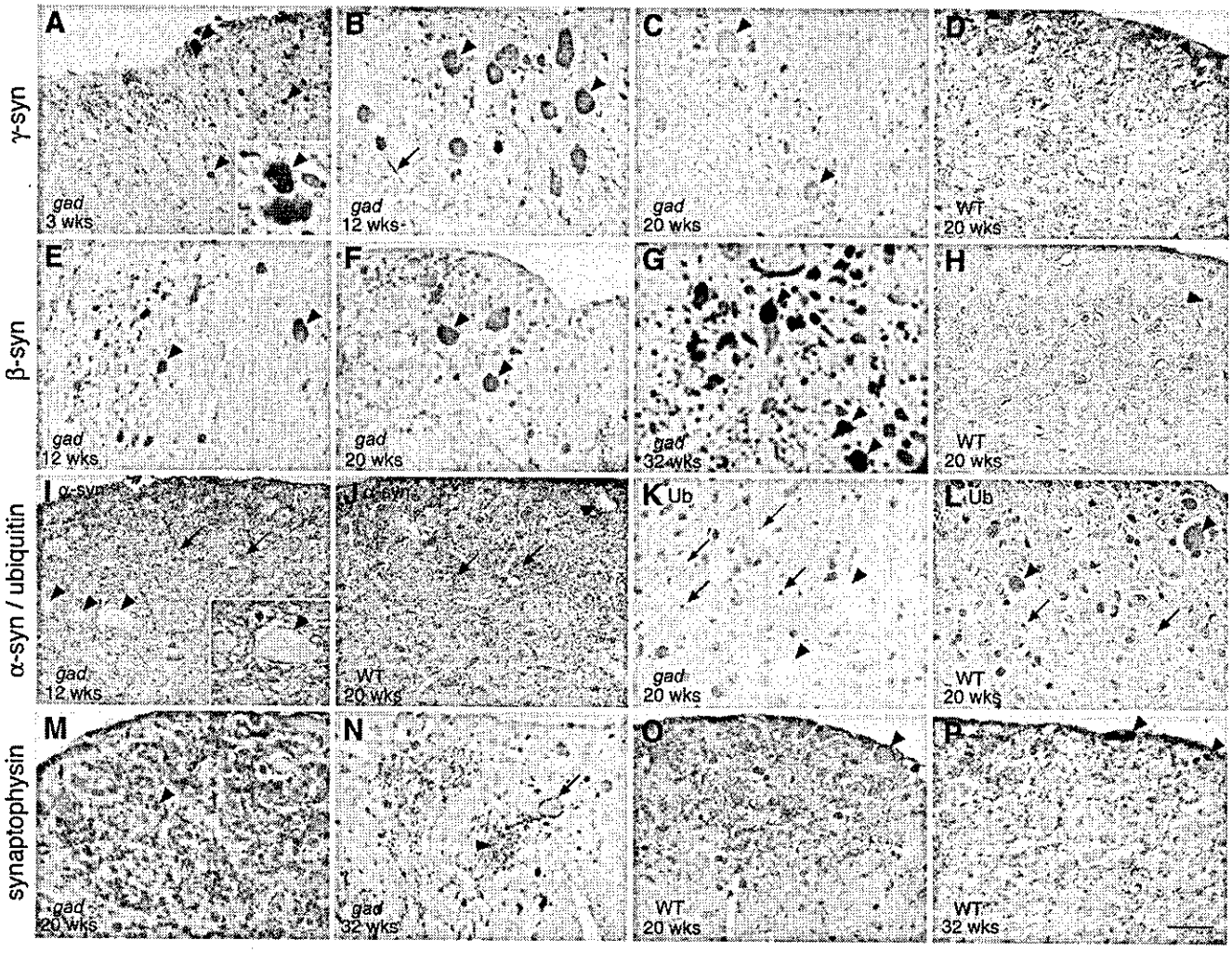

Fig. 4. Synucleins, synaptophysin and ubiquitin immunoreactivities of the gracile nucleus. Almost all spheroids showed strong immunostaining for (A–C) γ-syn and (E–G) β-syn in the gracile nucleus of gad mice from 3 to 32 weeks of age (A, 3 weeks; B and E, 12 weeks; C and F, 20 weeks; G, 32 weeks). Numerous γ-syn-positive spheroids (B, arrowheads) and occasional neurites (B, arrow) are demonstrated. Spheroids from wild-type mice at 20 weeks were also immunopositive for (D) γ-syn (arrowheads) and (H) β-syn (arrowhead). (I) Very little α-syn immunoreactivity was observed in *gad* mouse spheroids (12 weeks, arrowheads). (J) Also, as a positive control, there are any synaptic regions that could be indicated as being positive of α-syn in wild-type mouse (arrows) as well as in gad mouse (I, arrows), but α-syn was not detected in wild-type mouse spheroids (20 weeks, arrowheads). (K) Ubiquitin immunoreactivity in the *gad* mouse gracile nucleus (20 weeks) appeared in dots (arrows) but was not apparent in spheroids (arrowheads). (L) Ubiquitin-positive immunoreactivity was seen in both spheroids (arrowheads) and dots (arrows) in wild-type mice (20 weeks). For synaptophysin, except for the similar immunostaining pattern of synapses, the limited number of spheroids that were immunopositive exhibited diffuse or spotty staining (arrowheads) that was seen only in the center of spheroids at 20 weeks in both (M) *gad* and (0) wild-type mice. Indeed, *gad* mice had more synaptophysin immunoreactivity than did wild-type mice. (N) At 32 weeks, *gad* mice displayed a punctate distribution pattern of synaptophysin along synapses (arrowhead) or surrounding cell bodies, with a few densely stained spheroids (arrow). (P) In contrast, wild-type mice displayed an in situ expression pattern that was enriched in the spheroids at 32 weeks of age (arrowheads). Bar = 50 μm.

possible temporal relationships between spheroid formation and α-, β- and γ-synucleins in the *gad* mouse brain has not yet been proven. Because the *gad* mouse constitutes a neurodegenerative model for the study of spheroid proliferation in axonal termini, we therefore examined spheroid pathology using antibodies directed against α-, β- and γ-syn. Given that dystrophic swollen axons—the primary *gad* lesion observed in the gracile nucleus—result from spheroid proliferation, we quantitated spheroid formation and immunoreactivity in the medulla and upper cervical spinal cord regions over the lifetime of *gad* mice (Fig. 2F and Table 1).

We initially found that γ-syn-positive spheroids were more conspicuous than HE-stained spheroids during the early stage of age, suggesting that γ-syn is more sensitive and specific than HE for detecting spheroid formation in *gad* mice. β-syn was first detected in spheroids 8 weeks later than γ-syn. This result raises the possibility that the mechanism by which β-syn accumulates in spheroids differs from that of γ-syn and that γ-syn may play a more important role in the pathogenesis of the *gad* mutation. A recent study suggested that synucleins may help to regulate proteasome function by modulating 20S proteasome activity in the case

Table 1
Chronological change in the degree of immunoreactivity for spheroids stained for α-, β- and γ-synuclein and ubiquitin in the medulla and upper cervical cord of *gad* mice

	gad 3 weeks	*gad* 12 weeks	*gad* 20 weeks	*gad* 32 weeks	Wild-type 20 weeks	Wild-type 32 weeks
α-syn	−[a]	±	±	±	−	−
β-syn	−	+	++	+++	+	+
γ-syn	++	++	+++	+	+	+
ub-s[b]	−	−	−	−	+	+
ub-d[c]	−	++	+++	+	+	+

[a] Immunoreactivity: +++, strong; ++, moderate; + to ±, weaker to weak; −, not detectable.
[b] Ubiquitin immunoreactivity in the spheroids.
[c] Ubiquitin immunoreactivity in the dot-like structures.

of γ-syn and by affecting the 26S proteasome in the case of β-syn [34]. Thus, the fact that each of these two synucleins exhibits a distinct time course of spheroid accumulation may reflect differences in their metabolic regulation. Furthermore, γ-syn has a very different pattern of localization in neurons as compared with α-syn and β-syn [27].

Antibodies to ubiquitin recognize most spheroids, although it is unclear whether this recognition reflects sequestered free ubiquitin or ubiquitinated proteins [25,39]. Furthermore, the ubiquitinated substrates in spheroids have not been identified. We show here in *gad* mice that ubiquitin is absent from spheroids but is present in dot-like structures, which is consistent with a previous study [40]. Recently, we demonstrated that the loss of functional UCH-L1 leads to a decrease in free ubiquitin in *gad* mice [24]. In contrast, overexpression of UCH-L1 causes an increase in ubiquitin in both cultured cells and mice [24]. Therefore, we suggest that UCH-L1 ensures ubiquitin stability via prolonging the ubiquitin half-life within neurons as an important carrier protein, and loss of functional UCH-L1 may thus lead to inadequate ubiquitination via a decrease in free ubiquitin. Thus, the reduction in ubiquitin might be responsible for the absence of ubiquitin in *gad* mouse spheroids. Ubiquitin is, however, often detected in spheroid bodies during neurodegenerative diseases [2,41]. In addition, an increase in ubiquitin expression was reported in spheroid bodies in the brains of aged monkeys [31]. Despite the presence of ubiquitin in spheroid bodies in these systems, our data indicate that ubiquitination may not be required for the formation of spheroid bodies.

We found that spheroids were positive for both β- and γ-syn but were slight for α-syn in *gad* mice. Lewy bodies in PD and DLB brains are positive for both α-syn [36] and UCH-L1 [20], whereas we did not detect Lewy bodies or Lewy neurites in *gad* mouse brain. These observations suggest that the molecular mechanism of β- and γ-syn accumulation in *gad* spheroids is different from that in Lewy bodies. β-syn inhibits fibril accumulation of α-syn [11]. Thus, early accumulation of β-syn in the spheroids of *gad* mice may inhibit the accumulation of α-syn in spheroids or axon terminals. It remains unclear whether γ-syn has a similar effect on the accumulation of α-syn. Alternatively, fibril formation of α-syn might be affected by the existence of UCH-L1, and lack of UCH-L1 in the *gad* mouse might result in the suppression of α-syn aggregation in vivo. UCH-L1 was reported to have ubiquitin ligase activity that increased the amount of polyubiquitinated α-syn via K63-linked ubiquitination [19]. Other recent studies have shown that UCH-L1 can deubiquitinate polyubiquitinated α-syn with K48-linked ubiquitination [13,30]. Thus, a close relationship between UCH-L1 and α-syn has been implicated. Aggregates of β-syn and γ-syn have been found in dystrophic neurites associated with PD and other neurodegenerative diseases [7]. Neither protein, however, is detected in Lewy bodies in PD and DLB. Consequently, β-syn and γ-syn pathology may be more specific to spheroid disorders.

Pathological accumulations of β-syn and γ-syn were previously reported in neurological diseases [7]. β-syn is a presynaptic protein and *gad* degeneration starts at the presynapse of the gracile nuclei. Local accumulated β-syn may interfere with other presynaptic proteins in the degenerating terminals. We observed that a presynaptic protein, synaptophysin, was weakly detected in spheroids but strongly expressed in healthy synapses in *gad* mice. This result may support the idea of the effect of locally accumulated β-syn.

Overexpression of γ-syn may influence neurofilament network integrity [4]. Distinct from wild-type mice, in *gad* mice γ-syn immunoreactivity in the spheroids appeared in the gracile nucleus from an early stage, which might contribute to the dysfunction of the nervous system, possibly by interrupting axonal transport. Ubiquitin is known to be transported over long distances via slow axonal transport to synapses [3]. Ubiquitin reduction and the consequent inadequate ubiquitination of proteins may trigger accumulation of proteins that should undergo ubiquitin-dependent degradation. An age-dependent increase in γ- and β-syn-positive spheroids in *gad* mice resembles the accumulation of amyloid-β in spheroids of these mice [12]. Amyloid precursor protein has been shown to be transported by a fast axonal flow [16]. The abnormal accumulation of various proteins at terminals might affect axonal transport from the ganglia, leading to the dying-back type of degeneration of axons with formation of spheroid bodies. The mechanisms involved, however, will require more detailed studies of UCH-L1 and synucleins.

Acknowledgements

We thank Miss S. Kikuchi for assistance in preparation of the sections and Ms. M. Shikama for the care and breeding of animals. This work was supported in part by Grants-in-Aid for Scientific Research from the Ministry of Health, Labour and Welfare of Japan; Grants-in-Aid for Scientific Research from the Ministry of Education, Culture, Sports,

Science and Technology of Japan; a grant from the Organization for Pharmaceutical Safety and Research; and a grant from the Japan Science and Technology Agency.

References

[1] J. Aicardi, P. Castelein, Infantile neuroaxonal dystrophy, Brain 102 (1979) 727–748.

[2] N. Arai, Grumose or foamy spheroid bodies involving astrocytes in the human brain, Neuropathol. Appl. Neurobiol. 21 (1995) 238–245.

[3] A. Bizzi, B. Schaetzle, A. Patton, P. Gambetti, L. Autilio-Gambetti, Axonal transport of two major components of the ubiquitin system: free ubiquitin and ubiquitin carboxyl-terminal hydrolase PGP 9.5, Brain Res. 548 (1991) 292–299.

[4] V.L. Buchman, J. Adu, L.G. Pinon, N.N. Ninkina, A.M. Davies, Persyn, a member of the synuclein family, influences neurofilament network integrity, Nat. Neurosci. 1 (1998) 101–103.

[5] V.L. Buchman, H.J. Hunter, L.G. Pinon, J. Thompson, E.M. Privalova, N.N. Ninkina, A.M. Davies, Persyn, a member of the synuclein family, has a distinct pattern of expression in the developing nervous system, J. Neurosci. 18 (1998) 9335–9341.

[6] M. Farrer, J. Kachergus, L. Forno, S. Lincoln, D.S. Wang, M. Hulihan, D. Maraganore, K. Gwinn-Hardy, Z. Wszolek, D. Dickson, J.W. Langston, Comparison of kindreds with parkinsonism and alpha-synuclein genomic multiplications, Ann. Neurol. 55 (2004) 174–179.

[7] J.E. Galvin, K. Uryu, V.M. Lee, J.Q. Trojanowski, Axon pathology in Parkinson's disease and Lewy body dementia hippocampus contains alpha-, beta-, and gamma-synuclein, Proc. Natl. Acad. Sci. U. S. A. 96 (1999) 13450–13455.

[8] J.E. Galvin, B. Giasson, H.I. Hurtig, V.M. Lee, J.Q. Trojanowski, Neurodegeneration with brain iron accumulation, type 1 is characterized by alpha-, beta-, and gamma-synuclein neuropathology, Am. J. Pathol. 157 (2000) 361–368.

[9] M. Goedert, M.G. Spillantini, Dewy body diseases and multiple system atrophy as alpha-synucleinopathies, Mol. Psychiatry 3 (1998) 462–465.

[10] W. Halliday, The nosology of Hallervorden-spatz disease, J. Neurol. Sci. 134 (1995) 84–91 (Suppl.).

[11] M. Hashimoto, E. Rockenstein, M. Mante, M. Mallory, E. Masliah, beta-synuclein inhibits alpha-synuclein aggregation: a possible role as an anti-parkinsonian factor, Neuron 32 (2001) 213–223.

[12] N. Ichihara, J. Wu, D.H. Chui, K. Yamazaki, T. Wakabayashi, T. Kikuchi, Axonal degeneration promotes abnormal accumulation of amyloid beta-protein in ascending gracile tract of gracile axonal dystrophy (GAD) mouse, Brain Res. 695 (1995) 173–178.

[13] Y. Imai, M. Soda, R. Takahashi, Parkin suppresses unfolded protein stress-induced cell death through its E3 ubiquitin-protein ligase activity, J. Biol. Chem. 275 (2000) 35661–35664.

[14] T. Kikuchi, M. Mukoyama, K. Yamazaki, H. Moriya, Axonal degeneration of ascending sensory neurons in gracile axonal dystrophy mutant mouse, Acta Neuropathol. (Berl.) 80 (1990) 145–151.

[15] Y. Kon, D. Endoh, T. Iwanaga, Expression of protein gene product 9.5, a neuronal ubiquitin C-terminal hydrolase, and its developing change in sertoli cells of mouse testis, Mol. Reprod. Dev. 54 (1999) 333–341.

[16] E.H. Koo, S.S. Sisodia, D.-R. Archer, L.J. Martin, A. Weidemann, K. Beyreuther, P. Fischer, C.L. Masters, D.L. Price, Precursor of amyloid protein in Alzheimer disease undergoes fast anterograde axonal transport, Proc. Natl. Acad. Sci. U. S. A. 87 (1990) 1561–1565.

[17] R. Kruger, W. Kuhn, T. Muller, D. Woitalla, M. Graeber, S. Kosel, H. Przuntek, J.T. Epplen, L. Schols, O. Riess, Ala30Pro mutation in the gene encoding alpha-synuclein in Parkinson's disease, Nat. Genet. 18 (1998) 106–108.

[18] C. Lavedan, E. Leroy, A. Dehejia, S. Buchholtz, A. Dutra, R.L. Nussbaum, M.H. Polymeropoulos, Identification, localization and characterization of the human gamma-synuclein gene, Hum. Genet. 103 (1998) 106–112.

[19] Y. Liu, L. Fallon, H.A. Lashuel, Z. Liu, P.T. Lansbury Jr., The UCH-L1 gene encodes two opposing enzymatic activities that affect alpha-synuclein degradation and Parkinson's disease susceptibility, Cell 111 (2002) 209–218.

[20] J. Lowe, H. McDermott, M. Landon, R.J. Mayer, K.D. Wilkinson, Ubiquitin carboxyl-terminal hydrolase (PGP 9.5) is selectively present in ubiquitinated inclusion bodies characteristic of human neurodegenerative diseases, J. Pathol. 161 (1990) 153–160.

[21] H. Miura, K. Oda, C. Endo, K. Yamazaki, H. Shibasaki, T. Kikuchi, Progressive degeneration of motor nerve terminals in GAD mutant mouse with hereditary sensory axonopathy, Neuropathol. Appl. Neurobiol. 19 (1993) 41–51.

[22] M. Mukoyama, K. Yamazaki, T. Kikuchi, T. Tomita, Neuropathology of gracile axonal dystrophy (GAD) mouse. An animal model of central distal axonopathy in primary sensory neurons, Acta Neuropathol. (Berl) 79 (1989) 294–299.

[23] K. Nishikawa, H. Li, R. Kawamura, H. Osaka, Y.L. Wang, Y. Hara, T. Hirokawa, Y. Manago, T. Amano, M. Noda, S. Aoki, K. Wada, Alterations of structure and hydrolase activity of parkinsonism-associated human ubiquitin carboxyl-terminal hydrolase L1 variants, Biochem. Biophys. Res. Commun. 304 (2003) 176–183.

[24] H. Osaka, Y.L. Wang, K. Takada, S. Takizawa, R. Setsuie, H. Li, Y. Sato, K. Nishikawa, Y.J. Sun, M. Sakurai, T. Harada, Y. Hara, I. Kimura, S. Chiba, K. Namikawa, H. Kiyama, M. Noda, S. Aoki, K. Wada, Ubiquitin carboxy-terminal hydrolase L1 binds to and stabilizes monoubiquitin in neuron, Hum. Mel. Genet. 12 (2003) 1945–1958.

[25] Y. Oya, H. Nakayasu, N. Fujita, K. Suzuki, Pathological study of mice with total deficiency of sphingolipid activator proteins (SAP knockout mice), Acta Neuropathol. (Berl.) 96 (1998) 29–40.

[26] M.H. Polymeropoulos, C. Lavedan, E. Leroy, S.E. Ide, A. Dehejia, A. Dutra, B. Pike, H. Root, J. Rubenstein, R. Boyer, E.S. Stenroos, S. Chandrasekharappa, A. Athanassiadou, T. Papapetropoulos, W.G. Johnson, A.M. Lazzarini, R.C. Duvoisin, G. Di Iorio, L.I. Golbe, R.L. Nussbaum, Mutation in the alpha-synuclein gene identified in families with Parkinson's disease, Science 276 (1997) 2045–2047.

[27] M.C. Quilty, W.P. Gai, D.L. Pountney, A.K. West, J.C. Vickers, Localization of alpha-, beta-, and gamma-synuclein during neuronal development and alterations associated with the neuronal response to axonal trauma, Exp. Neurol. 182 (2003) 195–207.

[28] K. Saigoh, Y.L. Wang, J.G. Suh, T. Yamanishi, Y. Sakai, H. Kiyosawa, T. Harada, N. Ichihara, S. Wakana, T. Kikuchi, K. Wada, Intragenic deletion in the gene encoding ubiquitin carboxy-terminal hydrolase in gad mice, Nat. Genet. 23 (1999) 47–51.

[29] K. Saito, T. Yokoyama, M. Okaniwa, S. Kamoshita, Neuropathology of chronic vitamin E deficiency in fatal familial intrahepatic cholestasis, Acta Neuropathol. (Berl) 58 (1982) 187–192.

[30] D.M. Sampathu, B.I. Giasson, A.C. Pawlyk, J.Q. Trojanowski, V.M. Lee, Ubiquitination of alpha-synuclein is not required for formation of pathological inclusions in alpha-synucleinopathies, Am. J. Pathol. 163 (2003) 91–100.

[31] C. Schultz, E.J. Dick, A.B. Cox, G.B. Hubbard, E. Braak, H. Braak, Expression of stress proteins alpha B-crystallin, ubiquitin, and hsp27 in pallido-nigral spheroids of aged rhesus monkeys, Neurobiol. Aging 22 (2001) 677–682.

[32] R. Sidman, J.B. Angevine, E.T. Pierce, Atlas of the Mouse Brain and Spinal Cord, Harvard Univ. Press, Cambridge, 1971.

[33] A.B. Singleton, M. Farrer, J. Johnson, A. Singleton, S. Hague, J. Kachergus, M. Hulihan, T. Peuralinna, A. Dutra, R. Nussbaum, S. Lincoln, A. Crawley, M. Hanson, D. Maraganore, C. Adler, M.R. Cookson, M. Muenter, M. Baptista, D. Miller, J. Blancato, J. Hardy, K. Gwinn-Hardy, Alpha-synuclein locus triplication causes Parkinson's disease, Science 302 (2003) 841.

[34] H.M. Synder, K. Mensah, I. Surgucheva, B. Festoff, A. Matouschek, A. Surguchov, B. Wolozin, Effect of alpha, beta and gamma synuclein

on the proteasomal pathways: 20S ubiquitin-independent, 26S ubiquitin-indenedent and 26S ubiquintin-dependent. Program No.132.8. Abstract viewer/Itinerary Planner. Society for Neuroscience, Washinton, DC, 2003.

[35] A. Takeda, M. Mallory, M. Sundsmo, W. Honer, L. Hansen, E. Masliah, Abnormal accumulation of NACP/alpha-synuclein in neurodegenerative disorders, Am. J. Pathol. 152 (1998) 367–372.

[36] A. Takeda, M. Hashimoto, M. Mallory, M. Sundsumo, L. Hansen, E. Masliah, C-terminal alpha-synuclein immunoreactivity in structures other than Lewy bodies in neurodegenerative disorders, Acta Neuropathol. (Berl.) 99 (2000) 296–304.

[37] P.H. Tu, J.E. Galvin, M. Baba, B. Giasson, T. Tomita, S. Leight, S. Nakajo, T. Iwatsubo, J.Q. Trojanowski, V.M. Lee, Glial cytoplasmic inclusions in white matter oligodendrocytes of multiple system atrophy brains contain insoluble alpha-synuclein, Ann. Neurol. 44 (1998) 415–422.

[38] K.D. Wilkinson, S. Deshpande, C.N. Larsen, Comparisons of neuronal (PGP 9.5) and non-neuronal ubiquitin C-terminal hydrolases, Biochem. Soc. Trans. 20 (1992) 631–637.

[39] D. Willwohl, M. Kettner, H. Braak, G.B. Hubbard, E.J. Dick Jr., A.B. Cox, C. Schultz, Pallido-nigral spheroids in nonhuman primates: accumulation of heat shock proteins in astroglial processes, Acta Neuropathol. (Berl) 103 (2002) 276–280.

[40] J. Wu, N. Ichihara, D.H. Chui, K. Yamazaki, T. Kikuchi, Abnormal ubiquitination of dystrophic axons in centralnervous system of gracile axonal dystrophy (gad) mutant mouse, Alzheimer's Res. 47 (1996) 163–168.

[41] T. Yamada, H. Akiyama, P.L. McGeer, Two types of spheroid bodies in the nigral neurons in Parkinson's disease, Can. J. Neurol. Sci. 18 (1991) 287–294.

[42] K. Yamazaki, N. Wakasugi, T. Tomita, T. Kikuchi, M. Mukoyama, K. Ando, Gracile axonal dystrophy (GAD), a new neurological mutant in the mouse, Proc. Soc. Exp. Biol. Med. 187 (1988) 209–215.

[43] K. Yamazaki, H. Moriya, T. Wakabayashi, T. Kikuchi, Substance β-like immunoreactivity in the gracile nucleus and fasciculus in old mice, Neurosci. Lett. 106 (1989) 258–260.

[44] K. Yamazaki, A. Kobayashi, A. Kumazawa, T. Wakabayashi, K. Takeki, Axonal degeneration in the central nervous system of gracile axonal dystroph (gad) mice progresses like in human spinocerebellar ataxias, Biomed. Res. 12 (1991) 143–148.

American Journal of Pathology, Vol. 165, No. 4, October 2004

Cell Injury, Repair, Aging and Apoptosis

Two Closely Related Ubiquitin C-Terminal Hydrolase Isozymes Function as Reciprocal Modulators of Germ Cell Apoptosis in Cryptorchid Testis

Jungkee Kwon,*† Yu-Lai Wang,* Rieko Setsuie,*‡ Satoshi Sekiguchi,† Yae Sato,*‡ Mikako Sakurai,*‡ Mami Noda,‡ Shunsuke Aoki,* Yasuhiro Yoshikawa,† and Keiji Wada*

From the Department of Degenerative Neurological Diseases, National Institute of Neuroscience, National Center of Neurology and Psychiatry, Kodaira, Tokyo; the Department of Biomedical Science,† Graduate School of Agricultural and Life Sciences, University of Tokyo, Tokyo; and the Laboratory of Pathophysiology,‡ Graduate School of Pharmaceutical Sciences, Kyushu University, Fukuoka, Japan*

The experimentally induced cryptorchid mouse model is useful for elucidating the *in vivo* molecular mechanism of germ cell apoptosis. Apoptosis, in general, is thought to be partly regulated by the ubiquitin-proteasome system. Here, we analyzed the function of two closely related members of the ubiquitin C-terminal hydrolase (UCH) family in testicular germ cell apoptosis experimentally induced by cryptorchidism. The two enzymes, UCH-L1 and UCH-L3, deubiquitinate ubiquitin-protein conjugates and control the cellular balance of ubiquitin. The testes of gracile axonal dystrophy (*gad*) mice, which lack UCH-L1, were resistant to cryptorchid stress-related injury and had reduced ubiquitin levels. The level of both anti-apoptotic (Bcl-2 family and XIAP) and prosurvival (pCREB and BDNF) proteins was significantly higher in *gad* mice after cryptorchid stress. In contrast, *Uchl3* knockout mice showed profound testicular atrophy and apoptotic germ cell loss after cryptorchid injury. Ubiquitin level was not significantly different between wild-type and *Uchl3* knockout mice, whereas the levels of Nedd8 and the apoptotic proteins p53, Bax, and caspase3 were elevated in *Uchl3* knockout mice. These results demonstrate that UCH-L1 and UCH-L3 function differentially to regulate the cellular levels of anti-apoptotic, prosurvival, and apoptotic proteins during testicular germ cell apoptosis. *(Am J Pathol 2004, 165:1367–1374)*

In the ubiquitin-proteasome system, the levels of poly- and monoubiquitin are strictly controlled by the balance of two groups of specific enzymes: ubiquitinating enzymes (E1, E2, and E3) and deubiquitinating enzymes (DUBs).[1,2] DUBs are subdivided into ubiquitin C-terminal hydrolases (UCHs) and ubiquitin-specific proteases (UBPs).[3,4] The genes for at least four UCHs, UCH-L1 and UCH-L3, UCH-L4, and UCH-L5, have been identified in mice.[5,6] Among them, UCH-L1 and UCH-L3 predominate; these isozymes have 52% amino acid identity and share significant structural similarity;[7] however, the distribution of these two isozymes is quite distinct in that UCH-L3 mRNA is expressed ubiquitously whereas UCH-L1 mRNA is selectively expressed in the testis/ovary and neuronal cells.[7–10] Despite the high-sequence homology, the *in vitro* hydrolytic activities of these two enzymes differ significantly. The activity (Kcat) of UCH-L3 is more than 200-fold higher than UCH-L1 when a fluorogenic ubiquitin substrate is used.[11] In addition to its relatively weak hydrolase activity, UCH-L1 exhibits dimerization-dependent ubiquityl ligase activity.[11] In contrast, UCH-L3 has little or no ligase activity compared with UCH-L1.[11] It was recently suggested that UCH-L1 has anti-proliferative activity in tumor cells, and that its expression is induced in response to tumor growth.[12] Furthermore, UCH-L1 associates with monoubiquitin and prolongs ubiquitin half-life in neurons.[13] Other work demonstrated that UCH-L3 binds to Nedd8 and subsequently processes its C-terminus.[14] Nedd8 is a small ubiquitin-like protein that shares with ubiquitin the ability to be conjugated to a lysine residue in a substrate protein.[15] Covalent conjugation of proteins by Nedd8 is an important form of the posttranscriptional modification and plays a critical role in many cellular processes.[16] These conju-

Supported by Grants-in-Aid for Scientific Research from the Ministry of Health, Labor, and Welfare of Japan; Grants-in-Aid for Scientific Research from the Ministry of Education, Culture, Sports, Science, and Technology of Japan; a grant from Pharmaceuticals and Medical Devices Agency of Japan; and a grant from Japan Science and Technology Agency.

Accepted for publication June 24, 2004.

Address reprint requests to Keiji Wada, Department of Degenerative Neurological Disease, National Institute of Neuroscience, National Center of Neurology and Psychiatry, Kodaira, Tokyo, 187-8502, Japan. E-mail: wada@ncnp.go.jp.

gates are regulated by a large number of deconjugating enzymes. This activity is unique to UCH-L3 because UCH-L1 is relatively weak to cleave the C terminus of Nedd8.[14–16] Collectively, these data suggest that the two mouse isozymes, UCH-L1 and UCH-L3, have distinct but overlapping functions. In addition, we recently found that *gad* mice, which lack UCH-L1 expression, show reduced retinal cell apoptosis in response to ischemia, suggesting that UCH-L1 may promote apoptosis.[17]

Our previous work focused on the possibility that UCH-L1 and UCH-L3 exhibit functional diversity during spermatogenesis. We showed that both UCH-L1 and UCH-L3 are strongly but reciprocally expressed in the testis during spermatogenesis,[18] suggesting that each isozyme may have a distinct function in the testis. To elucidate the pathophysiological roles of these two isozymes in the testis, our present work examines the extent of heat-induced stress using experimentally induced cryptorchidism in *Uchl3* knockout[7] and *gad* mice.[8] Normally, the testes are maintained in the scrotum at a temperature lower than that of the abdomen. Exposure of a testis to higher body temperature via experimentally induced cryptorchidism results in rapid degeneration of testicular germ cells.[19–22] Recent studies show that testicular germ cell degeneration in cryptorchid testes occurs via apoptosis, and that protein and lipid oxidation, along with p53 promote germ cell death.[23–25] The ubiquitin-proteasome system is required for the subsequent degradation of the damaged testicular germ cells.[26–28] Here, we show that both UCH-L1 and UCH-L3 have reciprocal functions in testicular germ cells during cryptorchid-induced apoptosis. Our data show that the absence of UCH-L1 causes resistance to cryptorchid-induced testicular germ cell apoptosis, and that the knockout of UCH-L3 promotes germ cell apoptosis after cryptorchid injury.

Materials and Methods

Animals

We used 8-week-old *Uchl3* knockout (C57BL/6J)[7,18] and *gad*[8,18,29] (CBA/RFM) male mice. *Uchl3* knockout mice were generated by the standard method using homologously recombinant ES cells, and the knockout line was back-crossed several times to C57BL/6J mice.[7] The *gad* mouse is an autosomal recessive mutant that was obtained by crossing CBA and RFM mice.[8] The *gad* line was maintained by intercrossing for more than 20 generations.[8,29] Both strains were maintained at our institute. Animal care and handling were in accordance with institutional regulations for animal care and were approved by the Animal Investigation Committee of the National Institute of Neuroscience, National Center of Neurology and Psychiatry, Tokyo, Japan.

Unilateral Experimental Cryptorchidism

Unilateral cryptorchidism was experimentally induced under pentobarbital anesthesia (Abbott Laboratories, North Chicago, IL).[20,22] Briefly, a midline abdominal incision was made, and the left testis was displaced from scrotum and fixed to the upper abdominal wall. The right testis remained in the scrotum as an intact control within the same animal. At 0, 4, 7, and 14 days after the operation, four control and four cryptorchid testes were harvested to determine testis weight.

Histological and Immunohistochemical Assessment of Testes

Testes were embedded in paraffin wax after fixation in 4% paraformaldehyde, sectioned at 4-μm thickness, and stained with hematoxylin and eosin.[29] Light microscopy was used for routine observations. For immunohistochemical staining, the sections were incubated with 10% goat serum for 1 hour at room temperature, followed by incubation overnight at 4°C with a rabbit polyclonal antibody against ubiquitin (1:500; DakoCytomation, Glostrup, Denmark) or Nedd8 (1:500; Alexis Biochemicals, San Diego, CA) diluted in phosphate-buffered saline (PBS) containing 1% bovine serum albumin. Sections were then incubated with fluorescein isothiocyanate-conjugated goat anti-rabbit IgG (1:200; Jackson ImmunoResearch, West Grove, PA) for 1 hour at room temperature and examined by confocal laser-scanning microscopy (Olympus, Tokyo, Japan).

Apoptotic cells in testicular tissues were identified by terminal deoxynucleotidyl transferase (TdT)-mediated nick-end labeling (TUNEL) using the DeadEnd Fluorimetric TUNEL system kit (Promega, Madison, WI) and the anti-PARP p85 fragment pAb (Promega) according to the manufacturer's instructions.

Quantitative Analysis of Apoptotic Germ Cells

The number of apoptotic cells was determined by counting the positively stained nuclei in 30 circular seminiferous tubule cross-sections per testis section.[23,29] The proportion of seminiferous tubules containing apoptotic germ cells was calculated by dividing the number of seminiferous tubules containing apoptotic cells by the total number of seminiferous tubules. The incidence of apoptotic cells per apoptotic cell-containing seminiferous tubule was categorized into three groups, defined as 1 to 5, 6 to 10, and >11 positive cells.

Western Blotting

Western blots were performed as previously reported.[8,18,29] Total protein (5 μg/lane) was subjected to sodium dodecyl sulfate-polyacrylamide gel electrophoresis using 15% gels (Perfect NT Gel; DRC, Japan). Proteins were electrophoretically transferred to polyvinylidene difluoride membranes (Bio-Rad, Hercules, CA) and blocked with 5% nonfat milk in TBS-T [50 mmol/L Tris base, pH 7.5, 150 mmol/L NaCl, 0.1% (w/v) Tween-20]. The membranes were incubated individually with one or more primary antibodies to UCH-L1 and UCH-L3 (1:1000; peptide antibodies[18]), Bcl-2, Bcl-xL, Bax, p53, and caspase-3, (1:1000; all from Cell Signaling Technology, Beverly, MA), phosphorylated cyclic AMP response element-binding protein (pCREB, 1:500; Upstate Biotech-

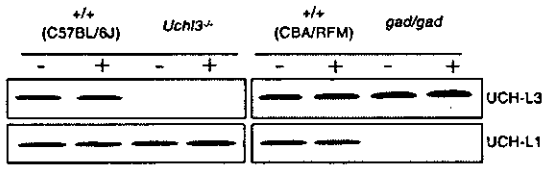

Figure 1. Western blotting analyses of both UCH-L3 and UCH-L1 in the testes of *gad* and *Uchl3* knockout mice, respectively, on day 4 after cryptorchid injury. Scrotal and cryptorchid testes did not differ significantly with respect to protein expression (−, scrotal testes; +, cryptorchid testes).

nology, Waltham, MA), brain-derived neurotrophic factor (BDNF, 1:500; Santa Cruz Biotechnology, Santa Cruz, CA), XIAP (1:500; Transduction Laboratories, Franklin Lakes, NJ), polyubiquitin (1:1000, clone FK-2; Medical & Biological Laboratories, Nagoya, Japan), monoubiquitin (1:1000, u5379; Sigma-Aldrich, St. Louis, MO), and Nedd8 (1:1000; Alexis Biochemicals, San Diego, CA). Blots were further incubated with peroxidase-conjugated goat anti-mouse IgG or goat anti-rabbit IgG (1:5000; Pierce, Rockford, IL) for 1 hour at room temperature. Immunoreactions were visualized using the SuperSignal West Dura extended duration substrate (Pierce) and analyzed with a Chemi-Imager (Alpha Innotech, San Leandro, CA). Each protein level was relatively quantificated after analysis with a ChemiImager using AlphaEase software.

Statistical Analysis

The mean and SD were calculated for all data (presented as mean ± SD). One-way analysis of variance was used for all statistical analyses.

Results

Level of Two UCH Isozymes in Scrotal and Cryptorchid Testes from Uchl3 Knockout and Gad Mice

We first confirmed the lack of UCH-L3 protein in the testes from *Uchl3* knockout mice by Western blotting (Figure 1). Similarly, we did not detect UCH-L1 protein in the testes of *gad* mice (Figure 1), as we previously observed.[13] Thus, in a biochemical sense, *gad* mice are analogous to *Uchl1*-null mice.[6,13] Compensatory level of UCH-L3 and UCH-L1 in *gad* and *Uchl3* knockout mice, respectively, was not observed (Figure 1; compare UCH-L3/UCH-L1 level with that of wild-type control mice). Experimental cryptorchidism did not affect UCH-L3 level in *gad* or wild-type control mice. Similarly, cryptorchidism did not affect UCH-L1 level in *Uchl3* knockout and wild-type control mice (Figure 1). Quantitative reverse transcriptase-polymerase chain reaction analysis showed that transcription from the *Uchl3* and *Uchl1* in both scrotal and cryptorchid testes from *gad* and *Uchl3* knockout mice was not significantly different from that measured in the corresponding wild-type control mice (data not shown). These results suggest that the level of UCH-L3 is regulated independently of UCH-L1 in the mouse testis, and that cryptorchid injury does not affect the level of either protein.

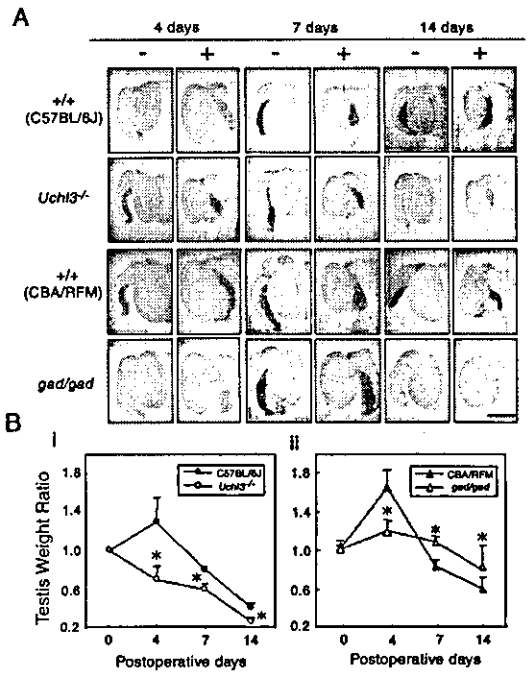

Figure 2. Comparison of testicular sizes and weights after experimental cryptorchidism. **A:** Gross images of changes in testicular size throughout time in two wild-type (C57BL/6J and CBA/RFM), *Uchl3* knockout, and *gad* mice (−, scrotal testes; +, cryptorchid testes). **B:** Ratio of cryptorchid to scrotal testis weight on days 0, 4, 7, and 14 after injury. i: Throughout time, the ratio for *Uchl3* knockout mice (**open circles**) differed significantly compared with wild-type mice (**filled circles**). ii: The ratio for *gad* mice (**open triangles**) did not differ significantly throughout time compared with wild-type mice (**closed triangles**). ($n = 4$; *, $P < 0.05$). Scale bar, 5 mm. Original magnifications, ×40.

Changes in Testicular Weight and Structure in Cryptorchid Uchl3 Knockout and Gad Mice

Unilateral cryptorchidism was surgically induced in *Uchl3* knockout and *gad* mice, and testes were evaluated on days 0, 4, 7, and 14 after the operation (Figure 2). Nonoperated (scrotal) testes served as controls for the evaluation of testicular weight and histochemistry. Cryptorchid testes from *Uchl3* knockout mice appeared smaller than the nonoperated controls at each time point, whereas the size of the cryptorchid testes from *gad* mice was similar to the controls (Figure 2A). Figure 2B shows the time course of the ratio of testicular weight of cryptorchid testes to scrotal testes. In wild-type mice (C57BL/6J and CBA/RFM), the ratio transiently increased 4 days after cryptorchid injury, most likely a consequence of inflammation-induced fluid accumulation[22,23] and biochemical changes observed. The ratio for these mice subsequently decreased below 1.0 by day 7. The ratio remained ~1.0 in *gad* mice (range,1.15 ~ 0.85), whereas it decreased significantly in *Uchl3* knockout mice compared with wild-type mice (Figure 2B). These results demonstrate that testes from *Uchl3* knockout and *gad* mice differ in their response to experimental cryptorchidism.

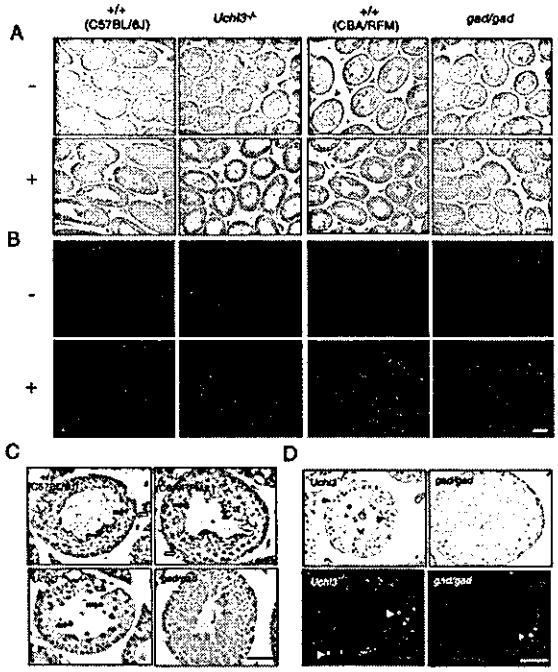

Figure 3. Histology and TUNEL staining of testicular cross sections after experimental cryptorchidism. **A:** Morphological analysis of seminiferous tubules on day 7 after cryptorchid injury. Note the germ cell loss and atrophy in cryptorchid testes compared with uninjured controls. (−, scrotal testes; +, cryptorchid testes). **B:** TUNEL staining of testicular cross-sections on day 7 after cryptorchid injury. Green fluorescence, TUNEL-positive cells; red fluorescence, nuclei stained with propidium iodide. **C:** Magnified cryptorchid testes sections. Pyknotic bodies (**filled arrows**) and Sertoli cell vacuolization (**open arrows**) were evident in cryptorchid testes of *Uchl3* knockout and the two wild-type (C57BL/6J and CBA/RFM) mice on day 7 after injury. **D:** PARP analysis to detect apoptotic germ cells in cryptorchid testes of *Uchl3* knockout and *gad* mice on day 7 after injury. The detection of apoptotic germ cells (**arrowheads, top**) by PARP analysis was consistent with that of apoptotic germ cells (**arrowheads, bottom**) by TUNEL analysis. Scale bar, 50 μm. Original magnifications: **A** and **B** ×100; **C** and **D** ×200.

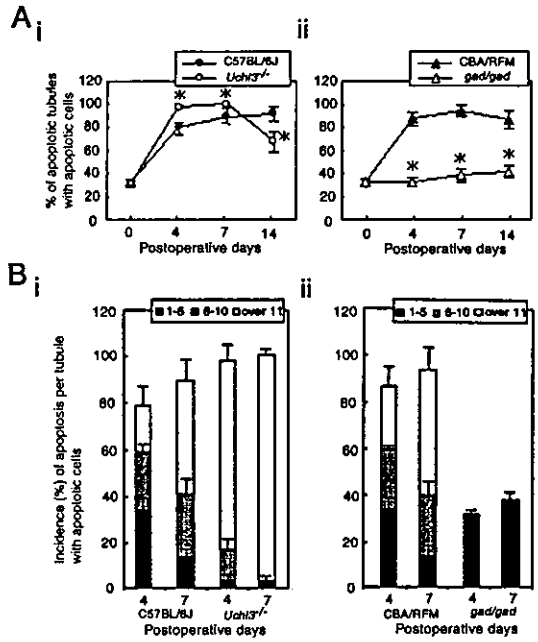

Figure 4. Quantitation of testicular germ cell apoptosis in testes after experimental cryptorchidism. **A:** The percentage of seminiferous tubules containing apoptotic germ cells in cryptorchid testes on days 0, 4, 7, and 14 after injury. **i:** The increase in the percentage of tubules containing apoptotic cells in the cryptorchid testes of *Uchl3* knockout mice is statistically significant compared with wild-type mice on days 4, 7, and 14. Each value represents the mean ± SD; *, $P < 0.05$. **ii:** The percentage of apoptotic tubules in cryptorchid testes of *gad* mice is significantly different on days 4, 7, and 14 after injury. Each value represents the mean ± SD; *, $P < 0.01$. **B:** Incidence of apoptosis per seminiferous tubule with apoptotic germ cells on days 4 and 7 after injury. The incidence of seminiferous tubules containing >11 apoptotic germ cells is significantly increased ($P < 0.05$) in cryptorchid testes of *Uchl3* knockout mice compared with wild-type mice. **i:** Comparison with *Uchl3* knockout mice. **ii:** Comparison with *gad* mice. Each value represents the mean ± SD.

Testicular Germ Cell Apoptosis in Cryptorchid Uchl3 Knockout and Gad Mice

To explore the mechanism underlying the observed differences between *Uchl3* knockout and *gad* cryptorchid testes, we prepared histological cross-sections on day 7 after testicular injury (Figure 3, A and C). The presence of nuclear pyknosis, multinucleated giant cells, and Sertoli cell vacuolization with germ cell loss in the germinal epithelium is indicative of cryptorchid testes.[22,23] These hallmarks of testicular injury were the most remarkable characteristics of cryptorchid testes from *Uchl3* knockout mice, demonstrating profound testicular atrophy and germ cell loss compared with wild-type mice (Figure 3, A and C). In contrast, no nuclear pyknosis, cellular shrinkage, or germ cell loss was observed in cryptorchid testes from *gad* mice. Spermatocytes and early spermatids comprised the majority of affected cell types in cryptorchid testes (Figure 3, A and C).

Germ cell apoptosis was further examined by TUNEL and PARP assays in tissue sections from postoperative day 7 mice (Figure 3, B and D). All but the *gad* cryptorchid testes showed a time-dependent increase in germ cell apoptosis during experimental cryptorchidism; germ cell apoptosis was always found in tubules that had germ cell loss on days 4, 7, and 14 (Figure 3, B and D, and Figure 4). Compared to wild-type mice, the cryptorchid testes of *Uchl3* knockout mice showed a marked increase in apoptotic germ cells in response to testicular injury, whereas *gad* mice lacked cryptorchid-induced germ cell apoptosis (Figure 3B and Figure 4). By postoperative days 4 and 7, the percentage of seminiferous tubules containing apoptotic germ cells increased with statistical significance ($n = 4$) ($P < 0.05$) in cryptorchid testes of *Uchl3* knockout mice as compared with wild-type mice (Figure 4A). In addition, cryptorchid testes of *Uchl3* knockout mice showed a high incidence of seminiferous tubules containing >11 apoptotic germ cells on days 4 and 7 days as compared with wild-type mice (Figure 4B); however, germ cell apoptosis did not increase in cryptorchid testes of *gad* mice during postoperative days 4 to 14 ($P < 0.01$) (Figure 4, A and B).

Cellular Mono- and Polyubiquitin Level in Cryptorchid Uchl3 Knockout and Gad Mice

Ubiquitin is required for energy-dependent degradation of structurally altered proteins.[26] We previously reported that UCH-L1 binds ubiquitin and stabilizes ubiquitin turnover in neurons, and that the level of monoubiquitin is decreased in *gad* mice.[13] In a model of ischemic insult in the retina, ubiquitin induction was unexpectedly lower and ischemic